# Electronic Supplementary Information

for

# Controlled Ring-Opening (Co)Polymerization of Macrolactones: A Pursuit for Efficient Aluminum-Based Catalysts

*Chutikan Nakornkhet,*[a,b] *Sirawan Kamavichanurat,*[a,b] *Wasan Joopor* [a,b] *and Pimpa Hormnirun*[a,b*]

[a] Laboratory of Catalysts and Advanced Polymer Materials, Department of Chemistry and Center of Excellence for Innovation in Chemistry, Faculty of Science, Kasetsart University, Bangkok 10900, Thailand

[b]Center for Advanced Studies in Nanotechnology for Chemical, Food and Agricultural Industries, Kasetsart University.

*E-mail: fscipph@ku.ac.th

## Content

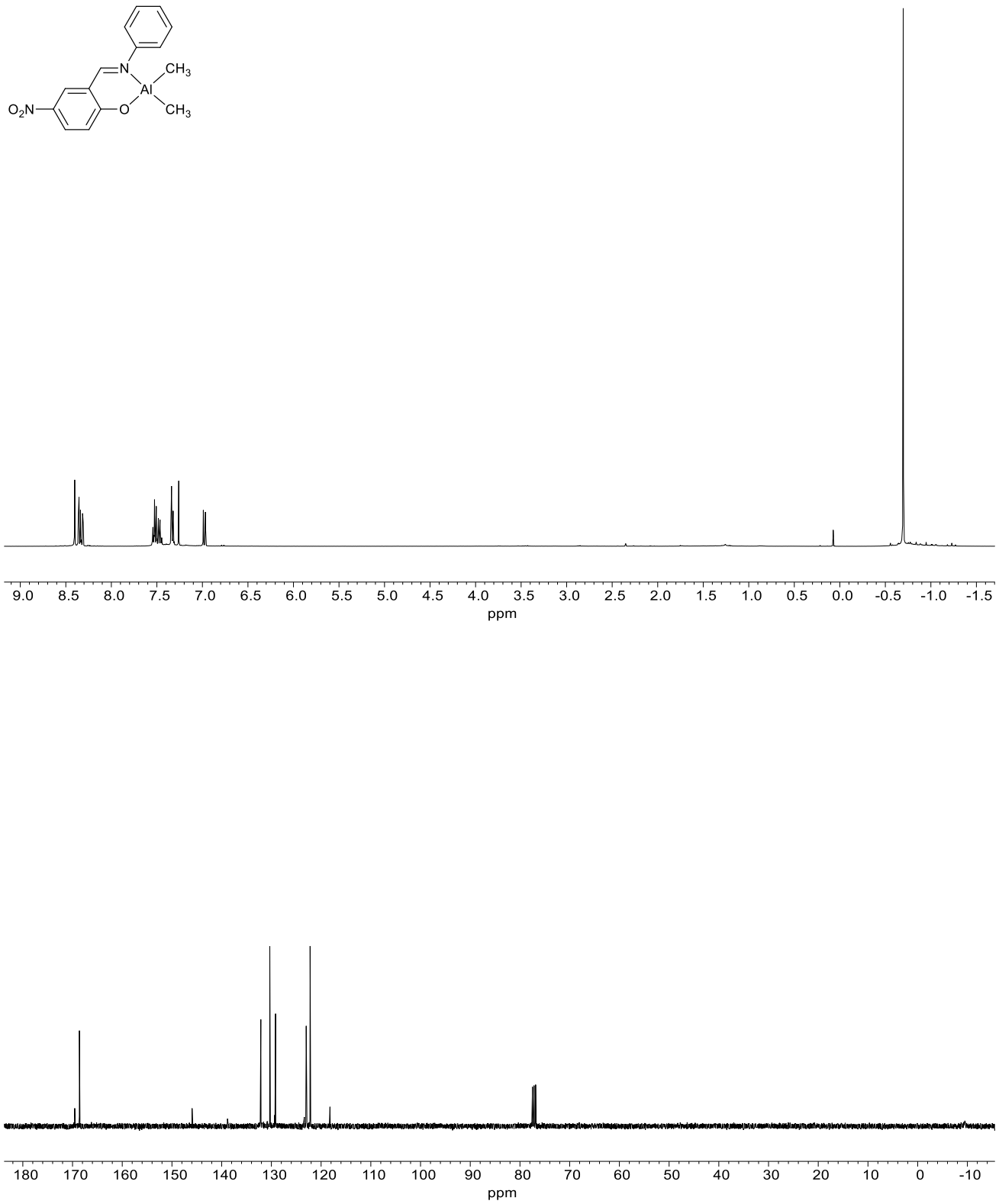


**Fig. S1** $^{1}H$ and $^{13}C\{^{1}H\}$ NMR spectra of **1** in $CDCl_3$ at 298 K.

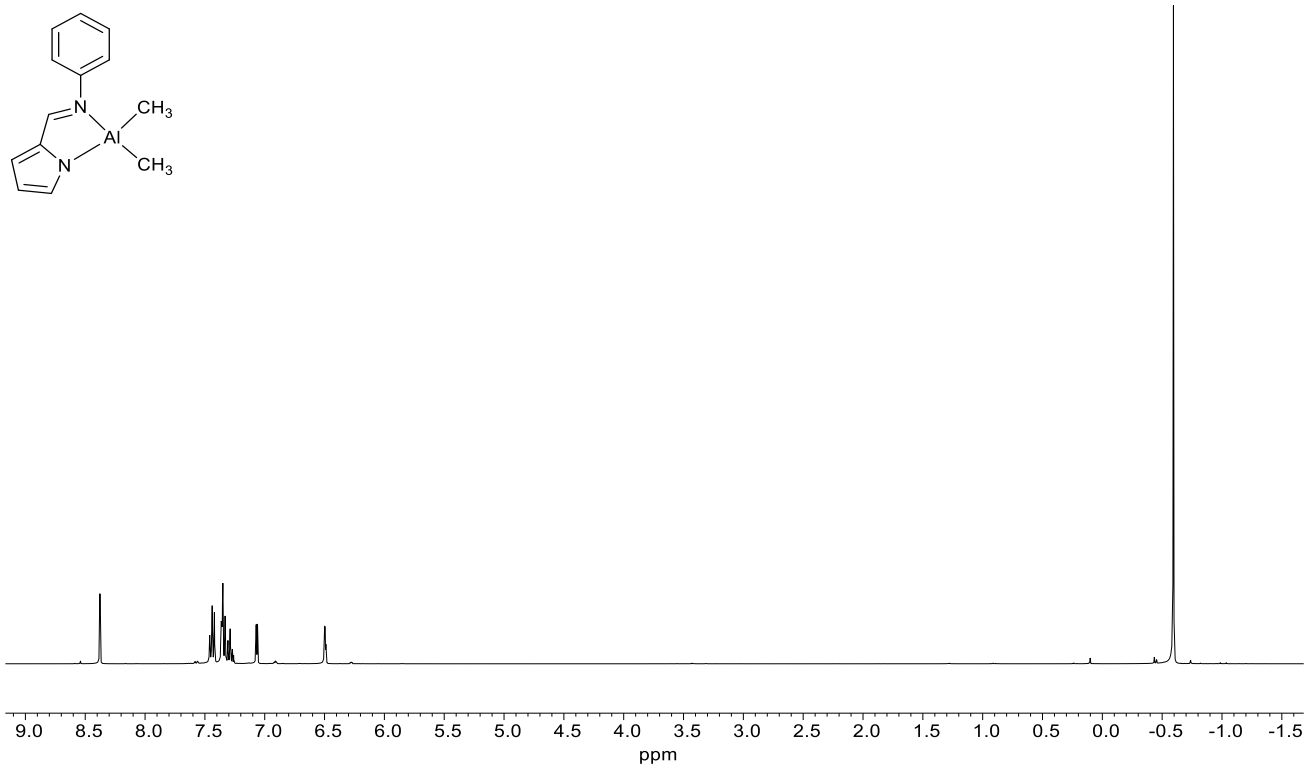


**Fig. S2** $^{1}$H NMR spectrum of **2** in $CDCl_3$ at 298 K.

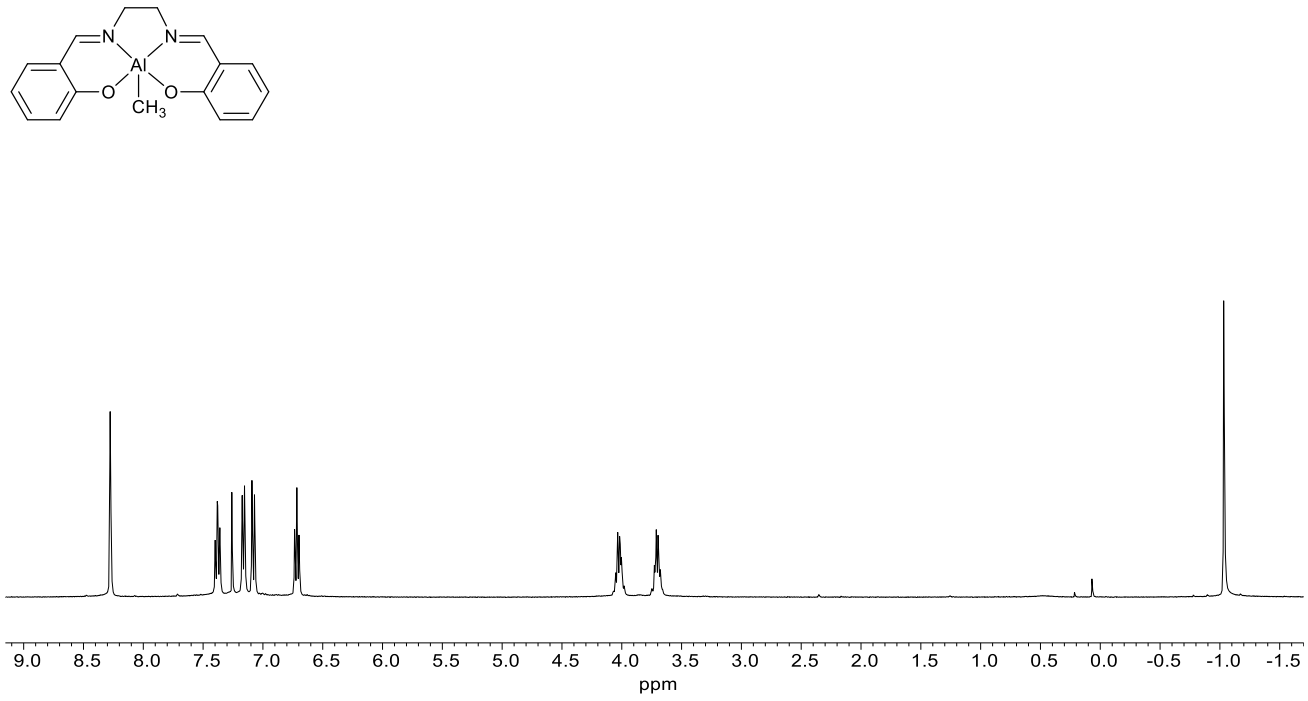


**Fig. S3** $^{1}$H NMR spectrum of **3** in $CDCl_3$ at 298 K.

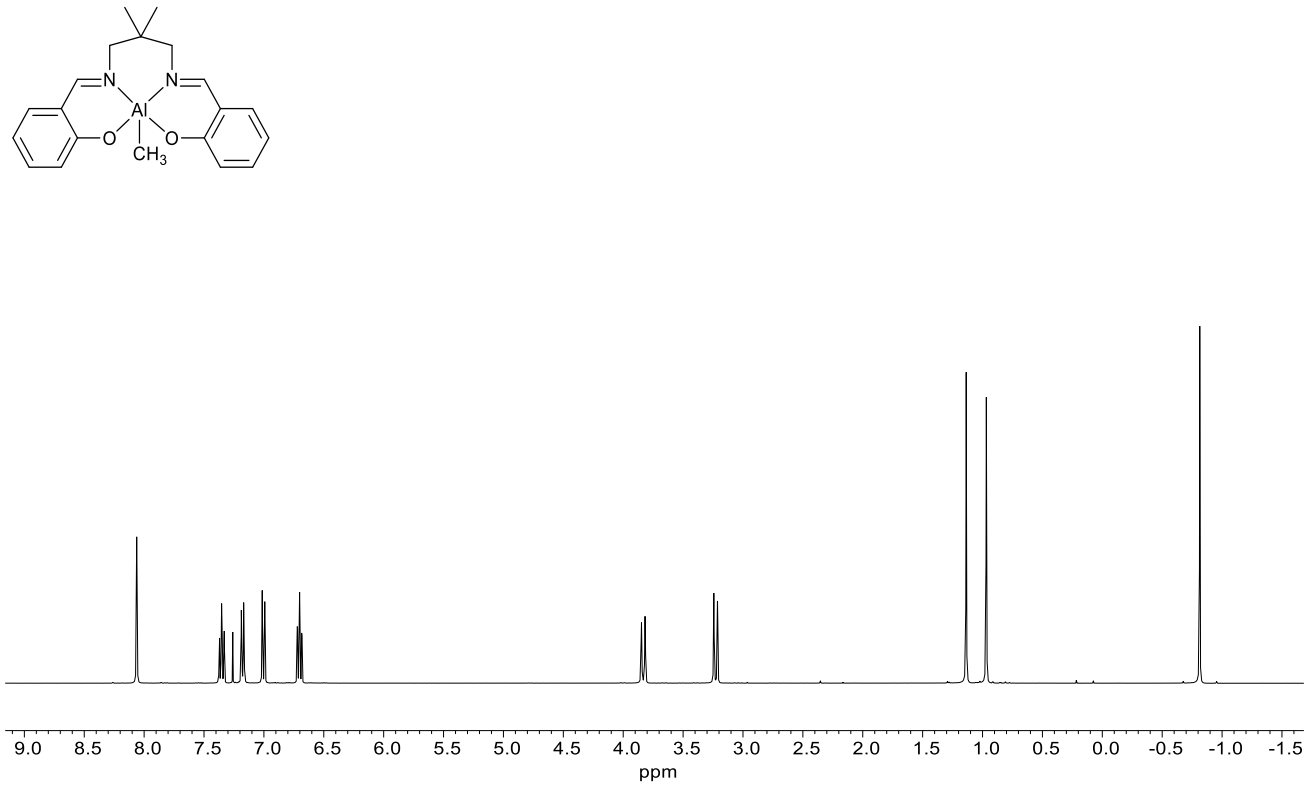


**Fig. S4** $^{1}$H NMR spectrum of **4** in $CDCl_3$ at 298 K.

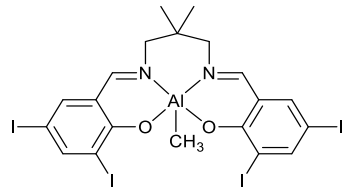


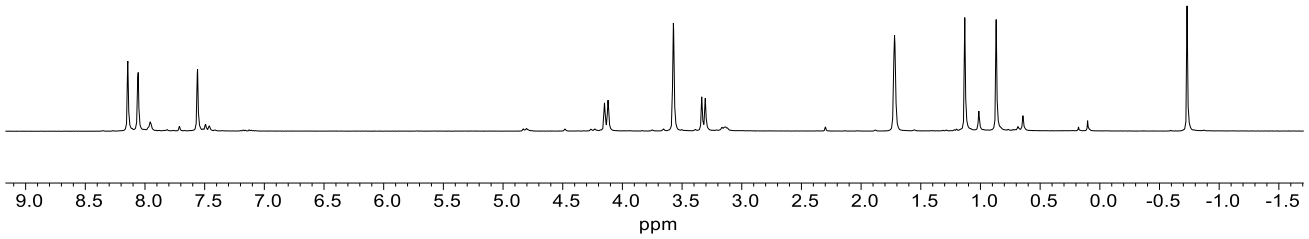


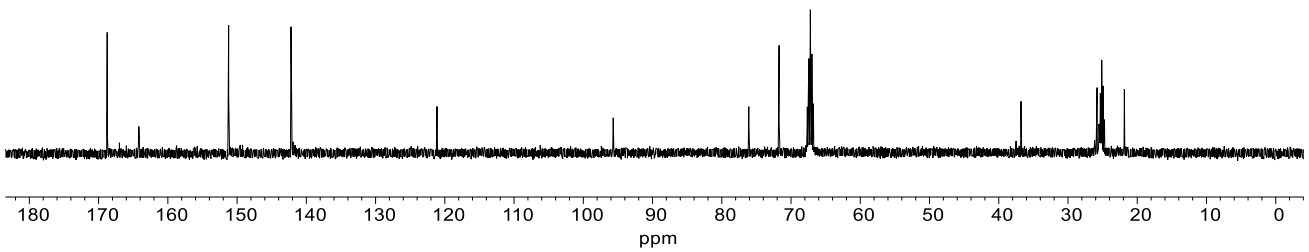


**Fig. S5** $^{1}H$ and $^{13}C\{^{1}H\}$ NMR spectra of **5** in THF-$d_8$ at 298 K.

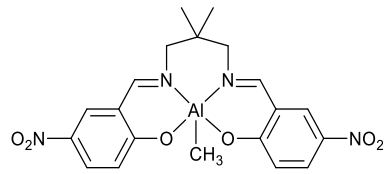


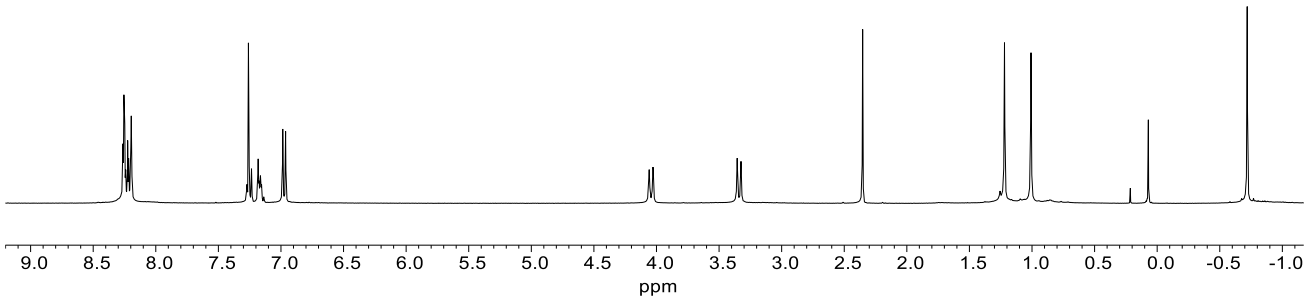


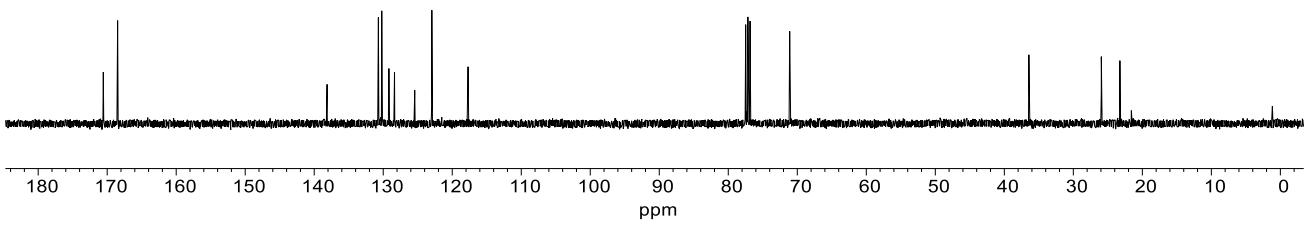


**Fig. S6** $^{1}H$ and $^{13}C\{^{1}H\}$ NMR spectra of **6** in $CDCl_3$ at 298 K.

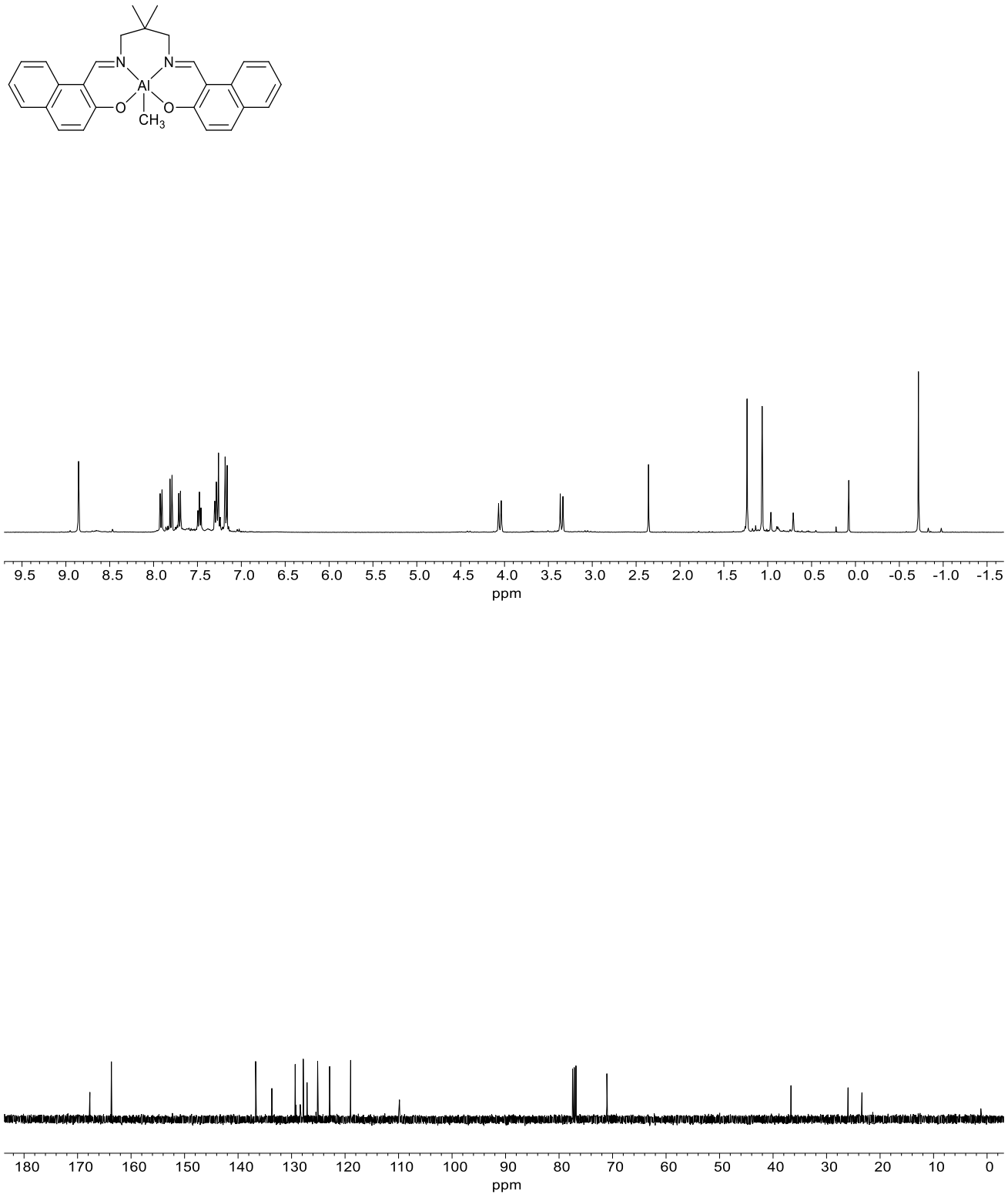


**Fig. S7** $^{1}H$ and $^{13}C\{^{1}H\}$ NMR spectra of **7** in $CDCl_3$ at 298 K.

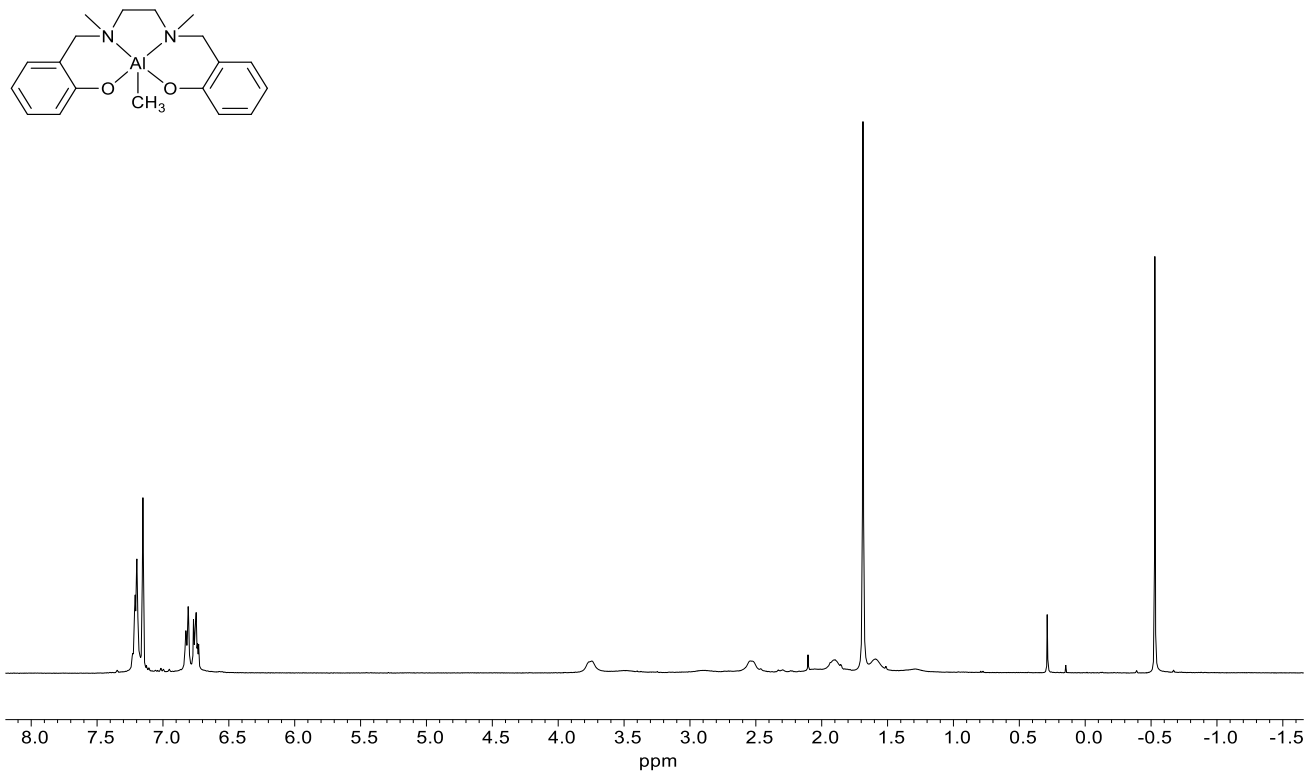


**Fig. S8** $^{1}$H NMR spectrum of **8** in $CDCl_3$ at 298 K.

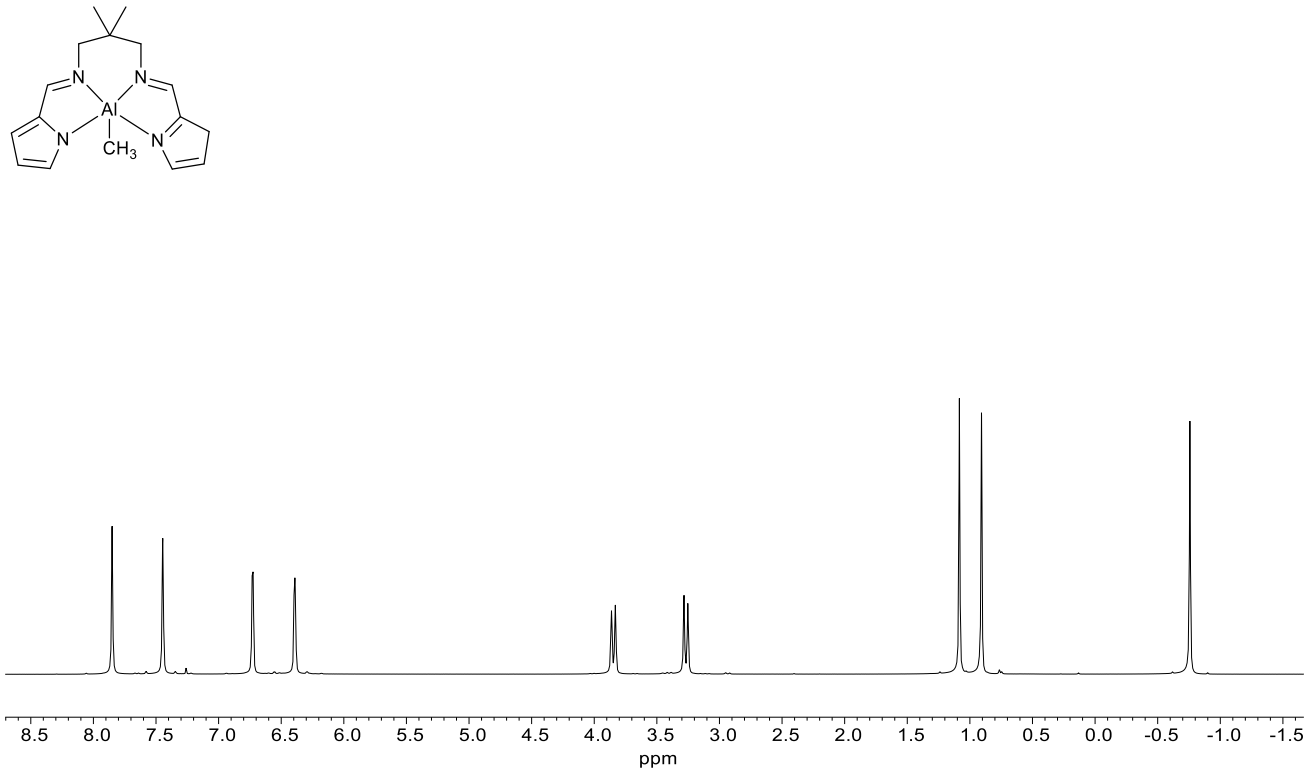


**Fig. S9** $^{1}$H NMR spectrum of **9** in $CDCl_3$ at 298 K.

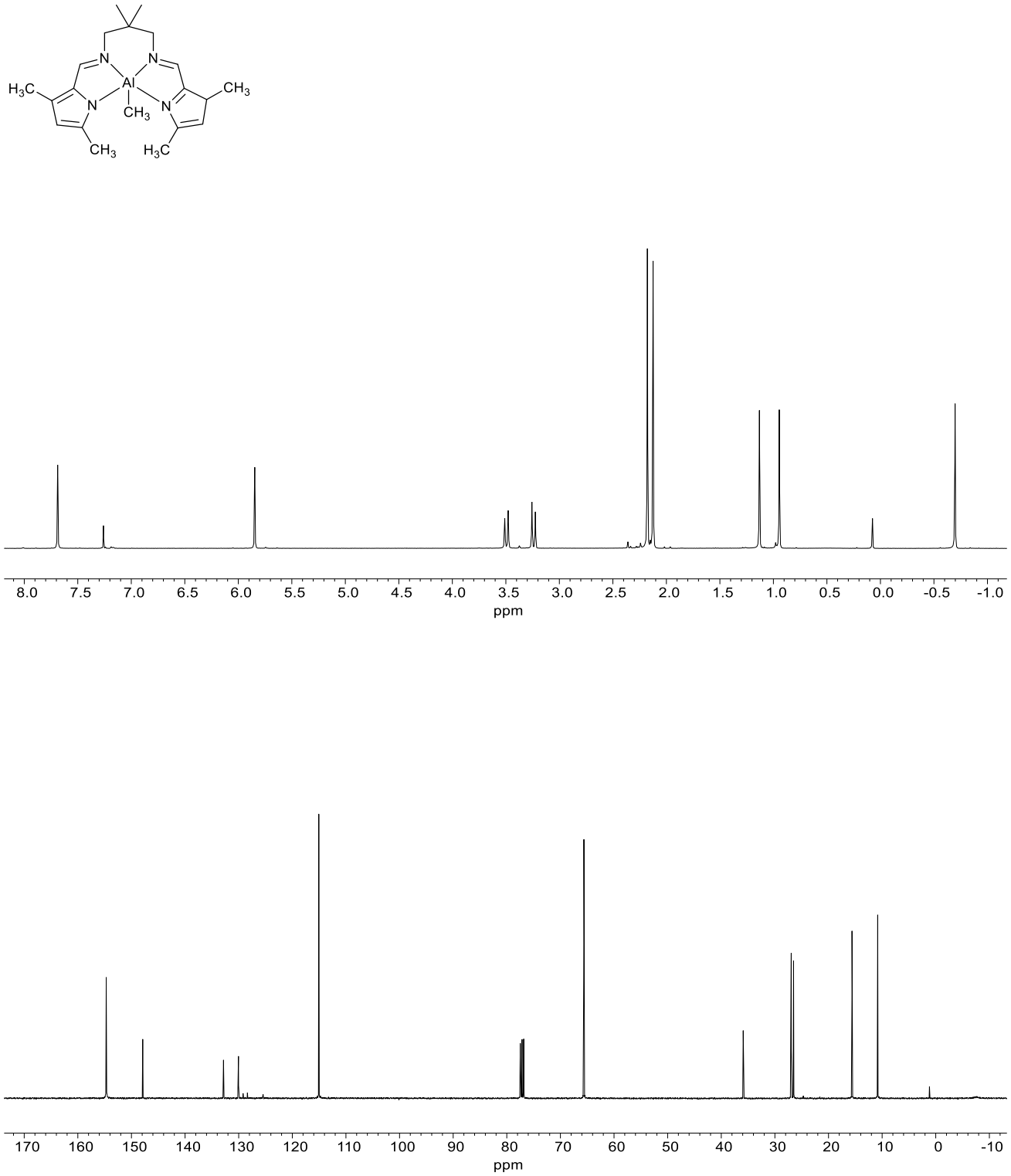


**Fig. S10** $^{1}H$ and $^{13}C\{^{1}H\}$ NMR spectra of **10** in $CDCl_3$ at 298 K.

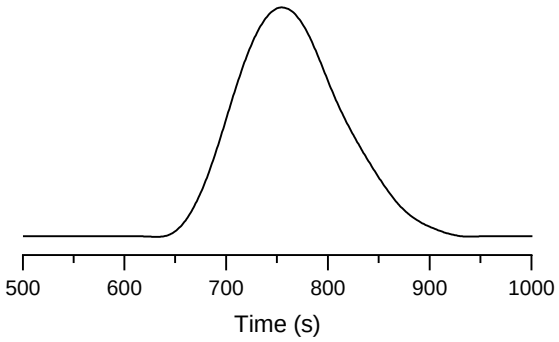


**Fig. S11** GPC trace of PPDL using complex **9** (Table 1, entry 9)

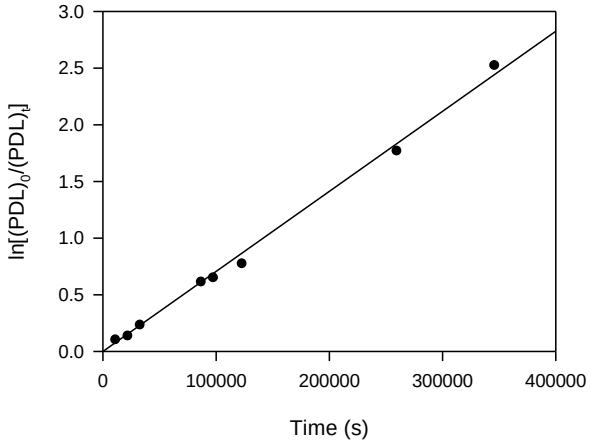


**Fig. S12** Semilogarithmic plot of PDL conversion versus time in $C_6D_6$ at 70 ºC with complex **1** ($[PDL]_0/[Al]$ = 100, [Al]/[BnOH] = 1, $[PDL]_0$ = 1.25, [Al] = 12.5 mM).

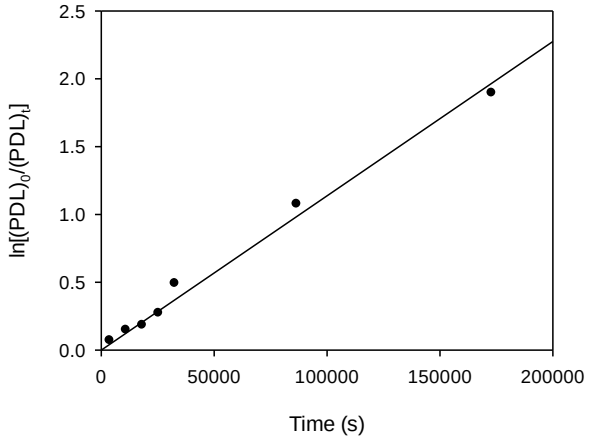


**Fig. S13** Semilogarithmic plot of PDL conversion versus time in $C_6D_6$ at 70 ºC with complex **2** ($[PDL]_0/[Al]$ = 100, [Al]/[BnOH] = 1, $[PDL]_0$ = 1.25, [Al] = 12.5 mM).

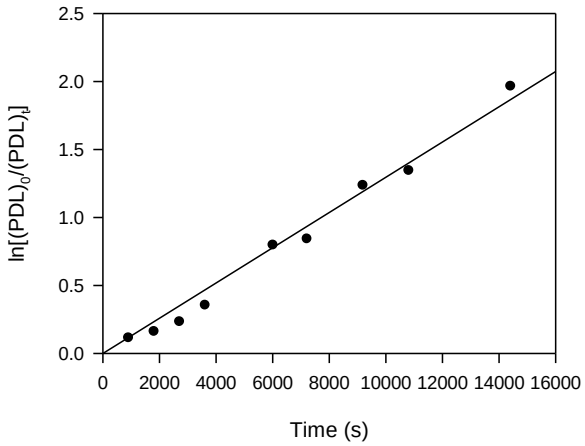


**Fig. S14** Semilogarithmic plot of PDL conversion versus time in $C_6D_6$ at 70 ºC with complex **3** ($[PDL]_0/[Al]$ = 100, [Al]/[BnOH] = 1, $[PDL]_0$ = 1.25, [Al] = 12.5 mM).

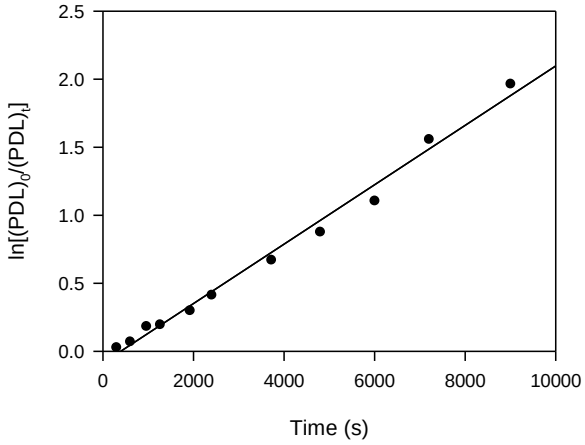


**Fig. S15** Semilogarithmic plot of PDL conversion versus time in $C_6D_6$ at 70 ºC with complex **4** ($[PDL]_0/[Al]$ = 100, [Al]/[BnOH] = 1, $[PDL]_0$ = 1.25, [Al] = 12.5 mM).

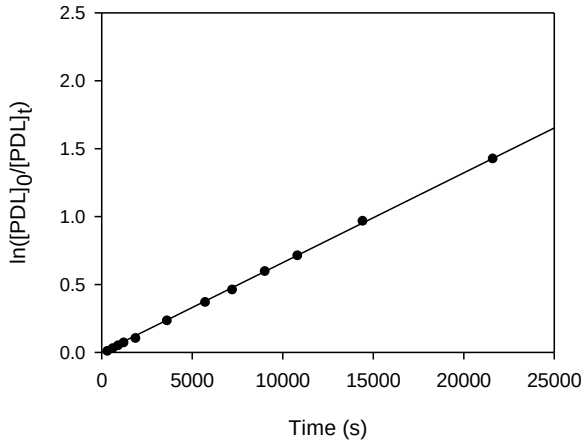


**Fig. S16** Semilogarithmic plot of PDL conversion versus time in $C_6D_6$ at 70 ºC with complex **5** ($[PDL]_0/[Al]$ = 100, [Al]/[BnOH] = 1, $[PDL]_0$ = 1.25, [Al] = 12.5 mM).

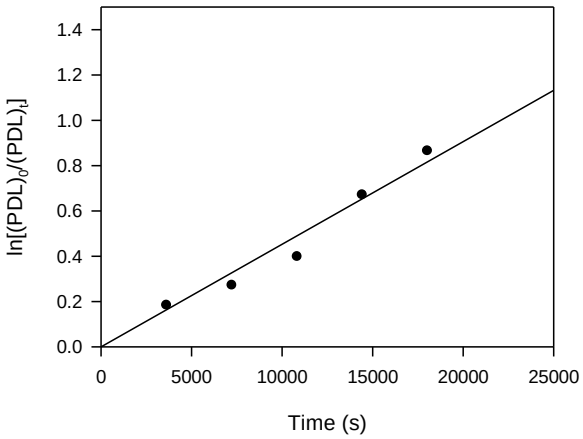


**Fig. S17** Semilogarithmic plot of PDL conversion versus time in $C_6D_6$ at 70 ºC with complex **6** ($[PDL]_0/[Al]$ = 100, [Al]/[BnOH] = 1, $[PDL]_0$ = 1.25, [Al] = 12.5 mM).

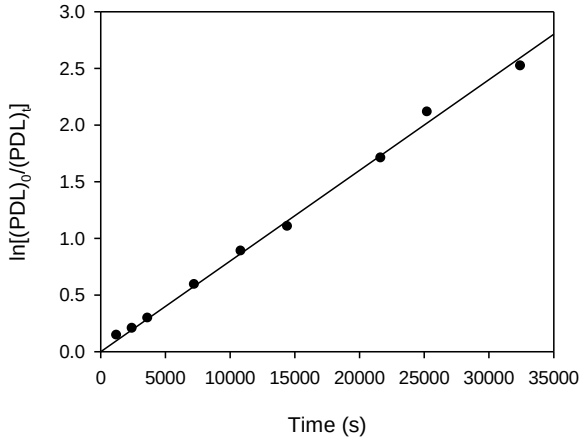


**Fig. S18** Semilogarithmic plot of PDL conversion versus time in $C_6D_6$ at 70 ºC with complex **7** ($[PDL]_0/[Al]$ = 100, [Al]/[BnOH] = 1, $[PDL]_0$ = 1.25, [Al] = 12.5 mM).

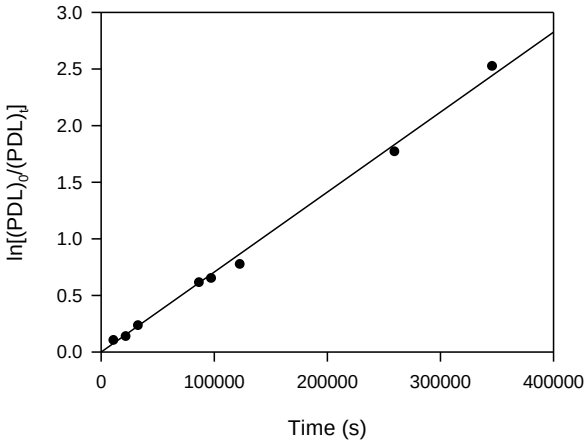


**Fig. S19** Semilogarithmic plot of PDL conversion versus time in $C_6D_6$ at 70 ºC with complex **8** ($[PDL]_0/[Al]$ = 100, [Al]/[BnOH] = 1, $[PDL]_0$ = 1.25, [Al] = 12.5 mM).

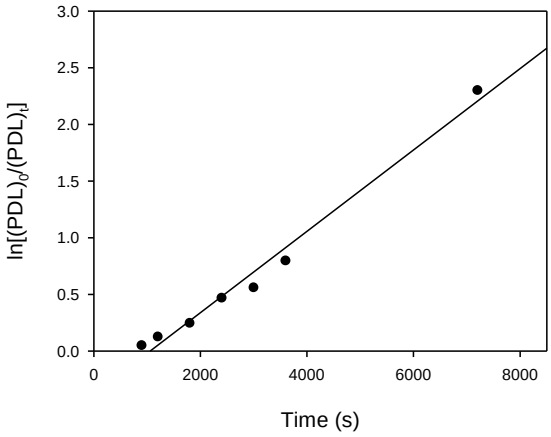


**Fig. S20** Semilogarithmic plot of PDL conversion versus time in $C_6D_6$ at 70 ºC with complex **9** ($[PDL]_0/[Al]$ = 100, [Al]/[BnOH] = 1, $[PDL]_0$ = 1.25, [Al] = 12.5 mM).

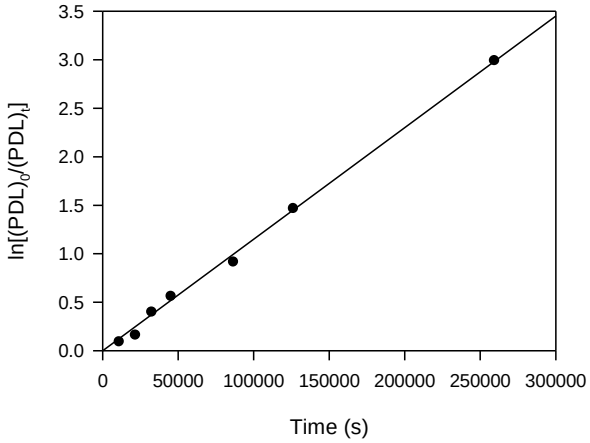


**Fig. S21** Semilogarithmic plot of PDL conversion versus time in $C_6D_6$ at 70 ºC with complex **10** ($[PDL]_0/[Al]$ = 100, [Al]/[BnOH] = 1, $[PDL]_0$ = 1.25, [Al] = 12.5 mM).

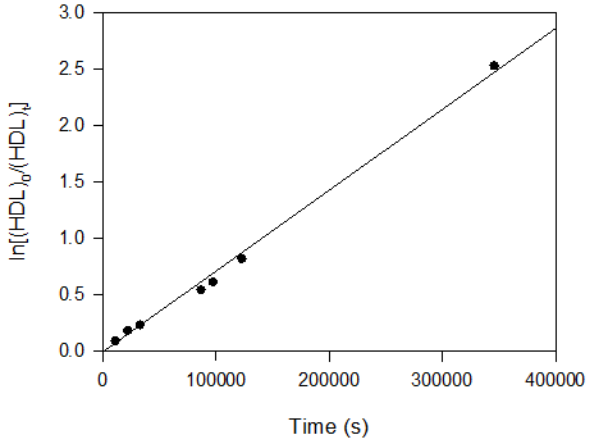


**Fig. S22** Semilogarithmic plot of HDL conversion versus time in $C_6D_6$ at 70 ºC with complex **1** ($[HDL]_0/[Al]$ = 100, [Al]/[BnOH] = 1, $[HDL]_0$ = 1.25, [Al] = 12.5 mM).

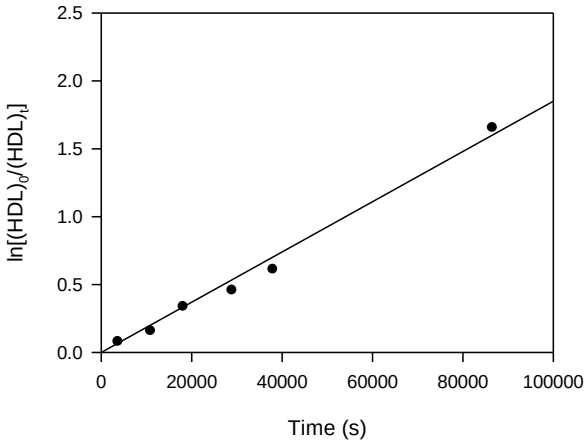


**Fig. S23** Semilogarithmic plot of HDL conversion versus time in $C_6D_6$ at 70 ºC with complex **2** ($[HDL]_0/[Al]$ = 100, [Al]/[BnOH] = 1, $[HDL]_0$ = 1.25, [Al] = 12.5 mM).

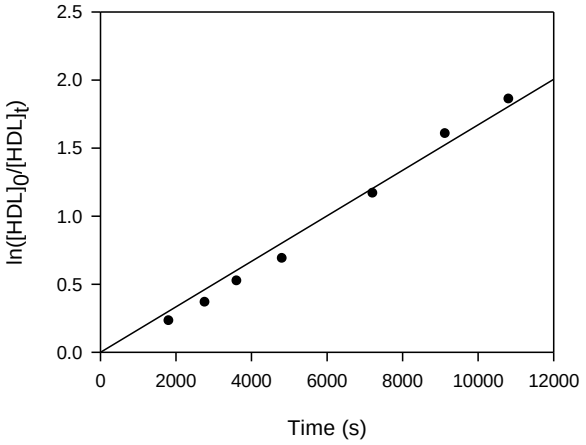


**Fig. S24** Semilogarithmic plot of HDL conversion versus time in $C_6D_6$ at 70 ºC with complex **3** ($[HDL]_0/[Al]$ = 100, [Al]/[BnOH] = 1, $[HDL]_0$ = 1.25, [Al] = 12.5 mM).

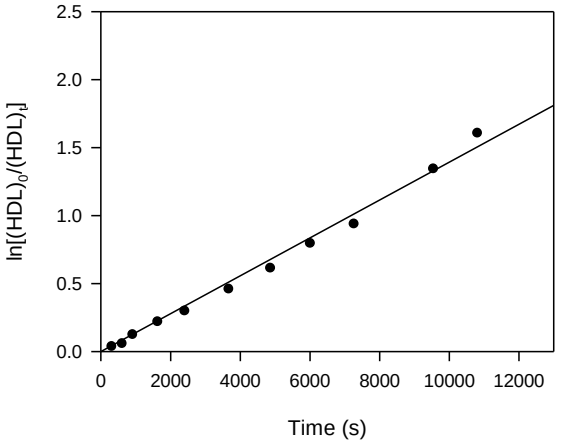


**Fig. S25** Semilogarithmic plot of HDL conversion versus time in $C_6D_6$ at 70 ºC with complex **4** ($[HDL]_0/[Al]$ = 100, [Al]/[BnOH] = 1, $[HDL]_0$ = 1.25, [Al] = 12.5 mM).

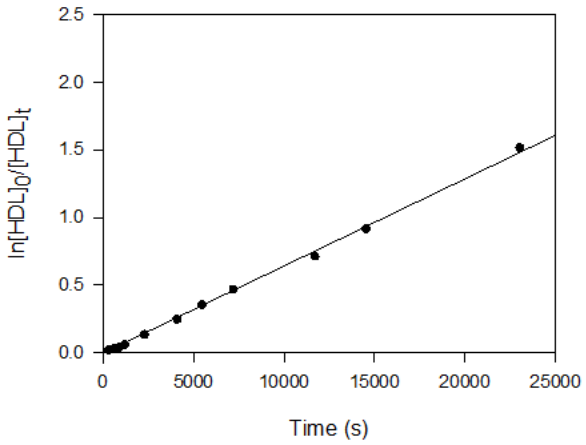


**Fig. S26** Semilogarithmic plot of HDL conversion versus time in $C_6D_6$ at 70 ºC with complex **5** ($[HDL]_0/[Al]$ = 100, [Al]/[BnOH] = 1, $[HDL]_0$ = 1.25, [Al] = 12.5 mM).

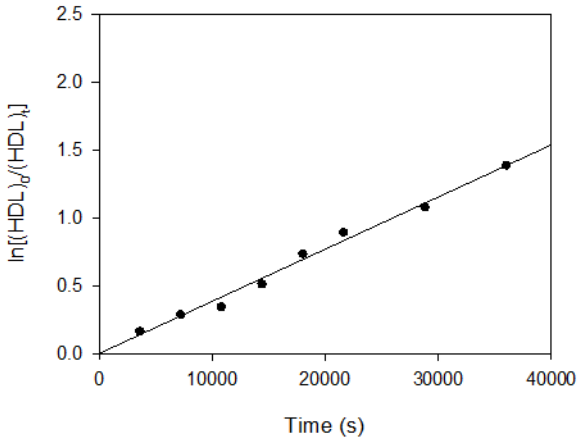


**Fig. S27** Semilogarithmic plot of HDL conversion versus time in $C_6D_6$ at 70 ºC with complex **6** ($[HDL]_0/[Al]$ = 100, [Al]/[BnOH] = 1, $[HDL]_0$ = 1.25, [Al] = 12.5 mM).

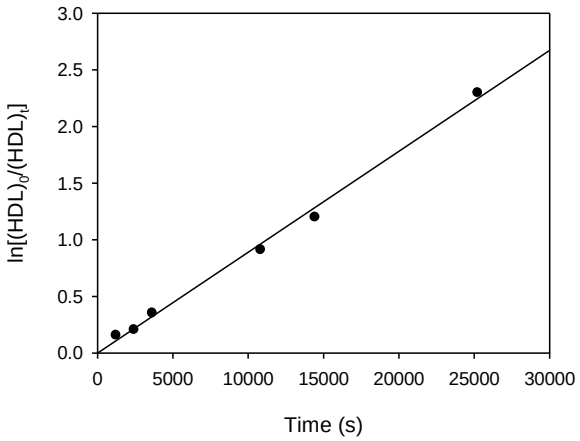


**Fig. S28** Semilogarithmic plot of HDL conversion versus time in $C_6D_6$ at 70 ºC with complex **7** ($[HDL]_0/[Al]$ = 100, [Al]/[BnOH] = 1, $[HDL]_0$ = 1.25, [Al] = 12.5 mM).

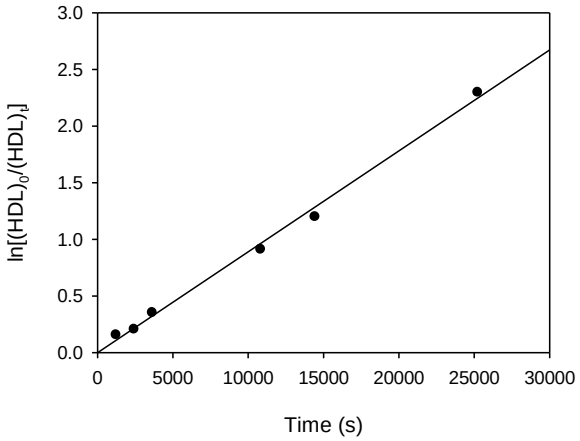


**Fig. S29** Semilogarithmic plot of HDL conversion versus time in $C_6D_6$ at 70 ºC with complex **8** ($[HDL]_0/[Al]$ = 100, $[Al]/[BnOH]$ = 1, $[HDL]_0$ = 1.25, [Al] = 12.5 mM).

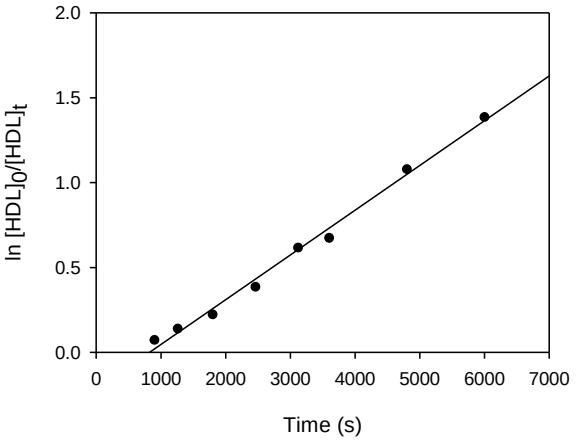


**Fig. S30** Semilogarithmic plot of HDL conversion versus time in $C_6D_6$ at 70 ºC with complex **9** ($[HDL]_0/[Al]$ = 100, $[Al]/[BnOH]$ = 1, $[HDL]_0$ = 1.25, [Al] = 12.5 mM).

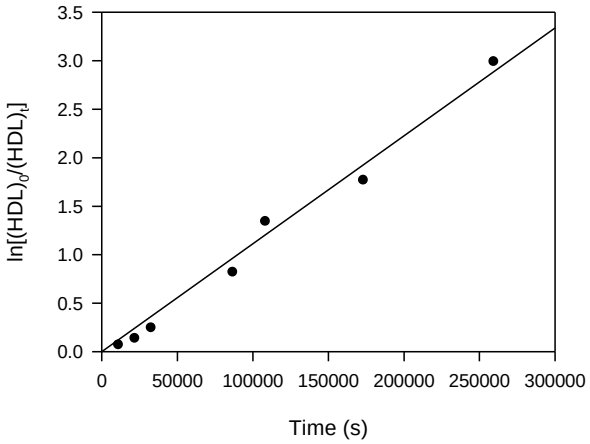


**Fig. S31** Semilogarithmic plot of HDL conversion versus time in $C_6D_6$ at 70 ºC with complex **10** ($[HDL]_0/[Al]$ = 100, $[Al]/[BnOH]$ = 1, $[HDL]_0$ = 1.25, [Al] = 12.5 mM).

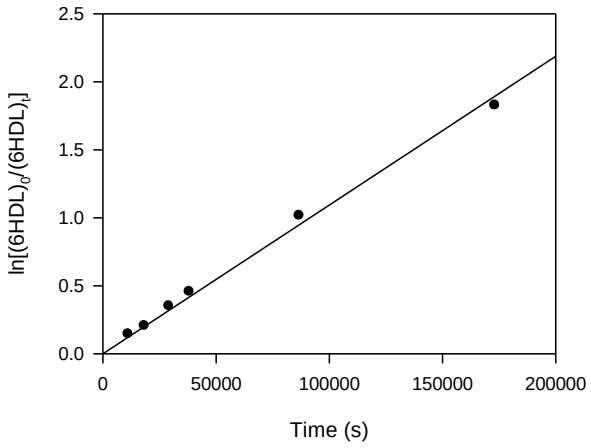


**Fig. S32** Semilogarithmic plot of 6HDL conversion versus time in $C_6D_6$ at 70 ºC with complex **1** ($[6HDL]_0/[Al] = 100$, $[Al]/[BnOH] = 1$, $[6HDL]_0 = 1.25$, $[Al] = 12.5$ mM).

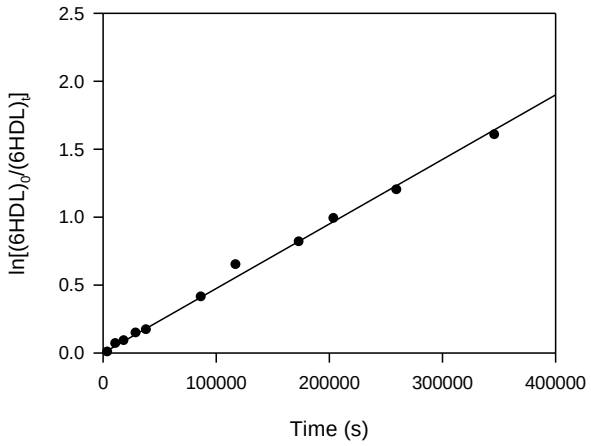


**Fig. S33** Semilogarithmic plot of 6HDL conversion versus time in $C_6D_6$ at 70 ºC with complex **2** ($[6HDL]_0/[Al] = 100$, $[Al]/[BnOH] = 1$, $[6HDL]_0 = 1.25$, $[Al] = 12.5$ mM).

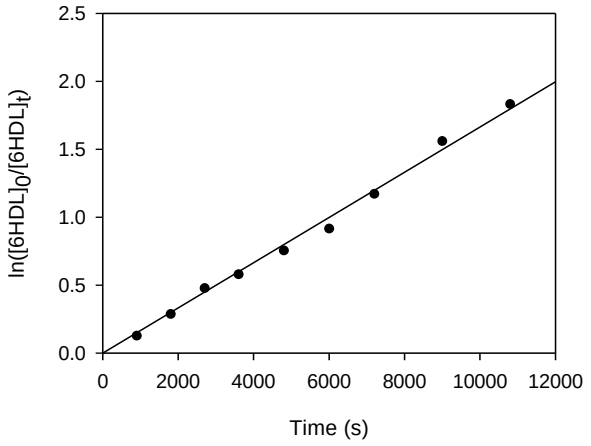


**Fig. S34** Semilogarithmic plot of 6HDL conversion versus time in $C_6D_6$ at 70 ºC with complex **3** ($[6HDL]_0/[Al] = 100$, $[Al]/[BnOH] = 1$, $[6HDL]_0 = 1.25$, $[Al] = 12.5$ mM).

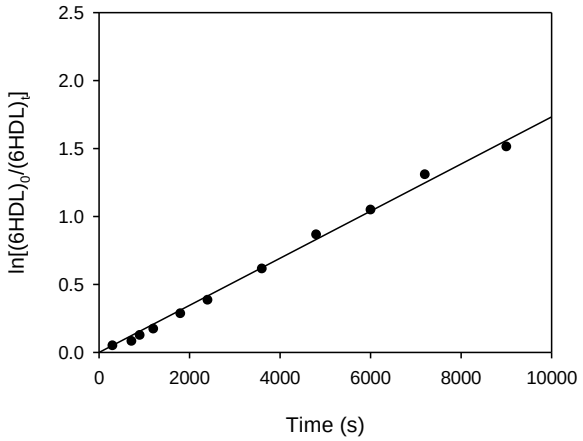


**Fig. S35** Semilogarithmic plot of 6HDL conversion versus time in $C_6D_6$ at 70 ºC with complex **4** ($[6HDL]_0/[Al]$ = 100, [Al]/[BnOH] = 1, $[6HDL]_0$ = 1.25, [Al] = 12.5 mM).

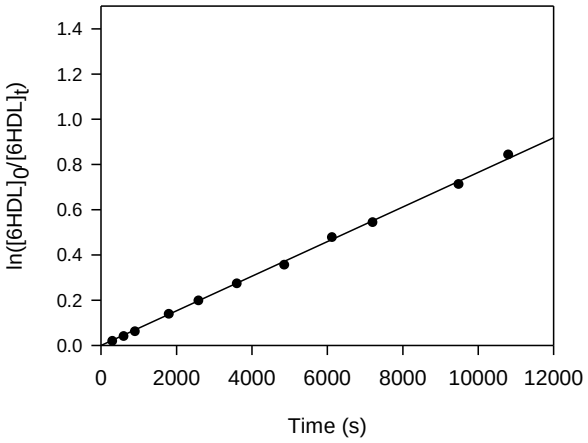


**Fig. S36** Semilogarithmic plot of 6HDL conversion versus time in $C_6D_6$ at 70 ºC with complex **5** ($[6HDL]_0/[Al]$ = 100, [Al]/[BnOH] = 1, $[6HDL]_0$ = 1.25, [Al] = 12.5 mM).

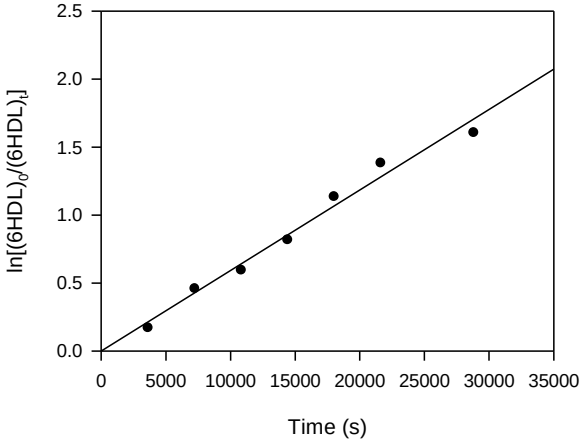


**Fig. S37** Semilogarithmic plot of 6HDL conversion versus time in $C_6D_6$ at 70 ºC with complex **6** ($[6HDL]_0/[Al]$ = 100, [Al]/[BnOH] = 1, $[6HDL]_0$ = 1.25, [Al] = 12.5 mM).

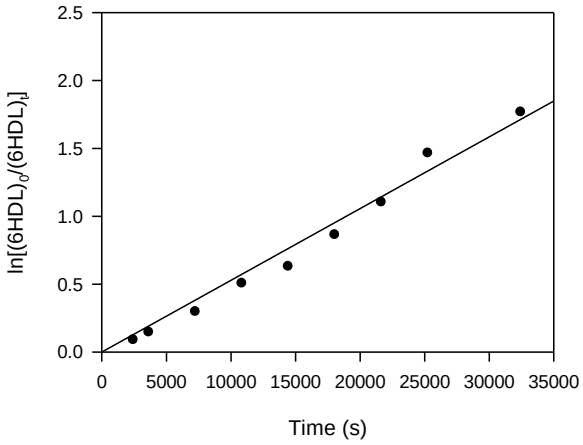


**Fig. S38** Semilogarithmic plot of 6HDL conversion versus time in $C_6D_6$ at 70 ºC with complex **7** ($[6HDL]_0/[Al]$ = 100, [Al]/[BnOH] = 1, $[6HDL]_0$ = 1.25, [Al] = 12.5 mM).

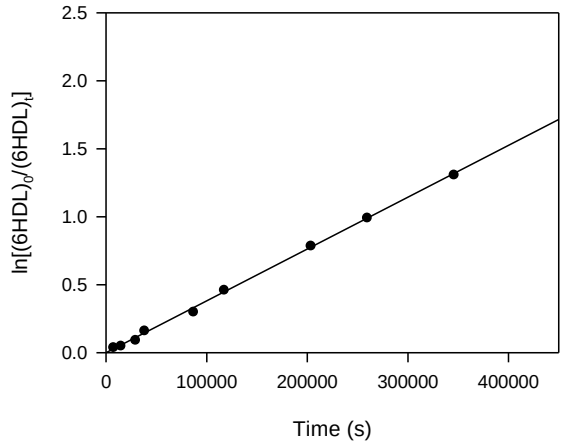


**Fig. S39** Semilogarithmic plot of 6HDL conversion versus time in $C_6D_6$ at 70 ºC with complex **8** ($[6HDL]_0/[Al]$ = 100, [Al]/[BnOH] = 1, $[6HDL]_0$ = 1.25, [Al] = 12.5 mM).

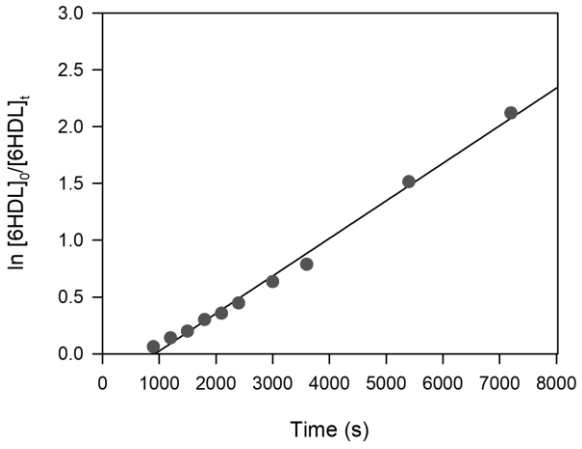


**Fig. S40** Semilogarithmic plot of 6HDL conversion versus time in $C_6D_6$ at 70 ºC with complex **9** ($[6HDL]_0/[Al]$ = 100, [Al]/[BnOH] = 1, $[6HDL]_0$ = 1.25, [Al] = 12.5 mM).

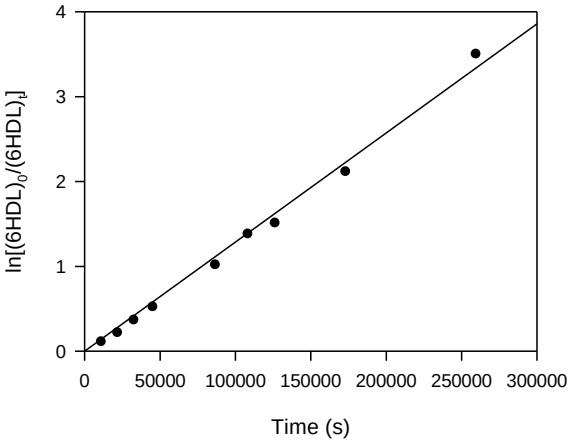


**Fig. S41** Semilogarithmic plot of 6HDL conversion versus time in $C_6D_6$ at 70 ºC with complex **10** ($[P6HDL]_0/[Al] = 100$, $[Al]/[BnOH] = 1$, $[6HDL]_0 = 1.25$, $[Al] = 12.5$ mM).

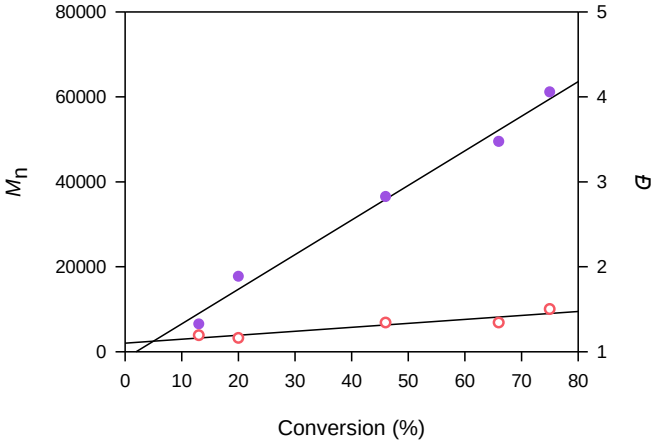


**Fig. S42** Plot of the HDL $M_n$ (●) (*versus* polystyrene standards) and $Đ$ (○) as a function of monomer conversion for HDL using **9**/BnOH as an initiator ($[HDL]_0/[Al] = 100$, $C_6D_6$, 70 °C).

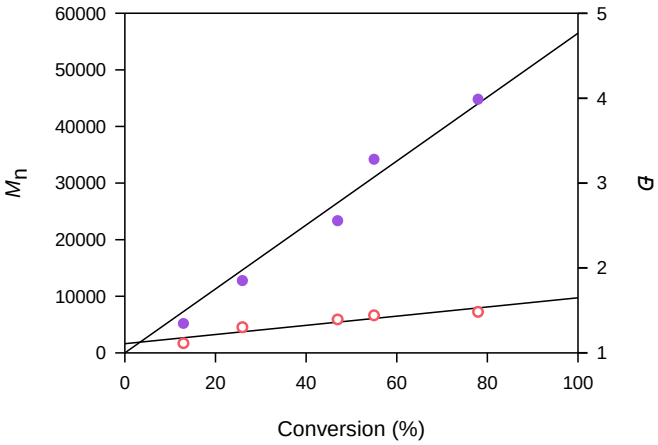


**Fig. S43** Plot of the 6HDL $M_n$ (●) (versus polystyrene standards) and PDI (○) as a function of monomer conversion for 6HDL using **9**/BnOH as an initiator ($[6HDL]_0/[Al] = 100$, $C_6D_6$, 70 °C).

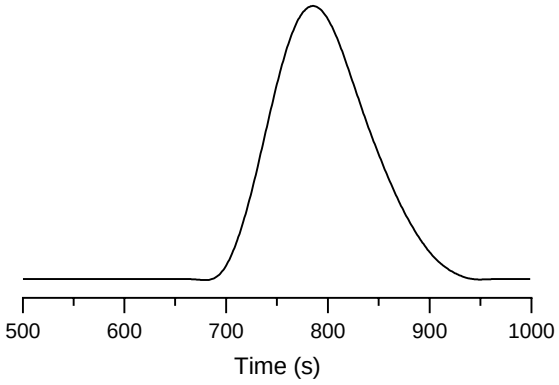


**Fig. S44** GPC curve of Poly(PDL-*b*-L-LA) using complex **9** (Table 6, entry 1)

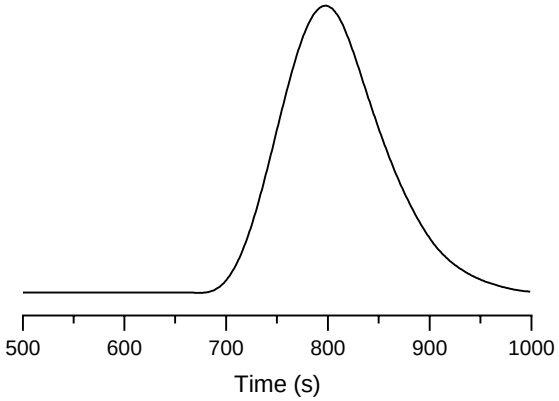


**Fig. S45** GPC curve of Poly(L-LA-*co*-PDL) using complex **9** (Table 6, entry 2)

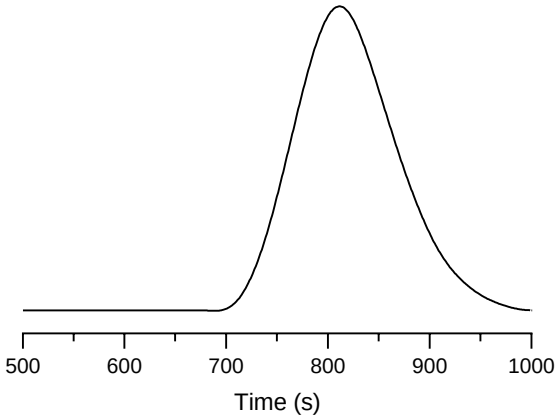


**Fig. S46** GPC curve of Poly(L-LA-*co*-PDL) using complex **9** (Table 6, entry 3)

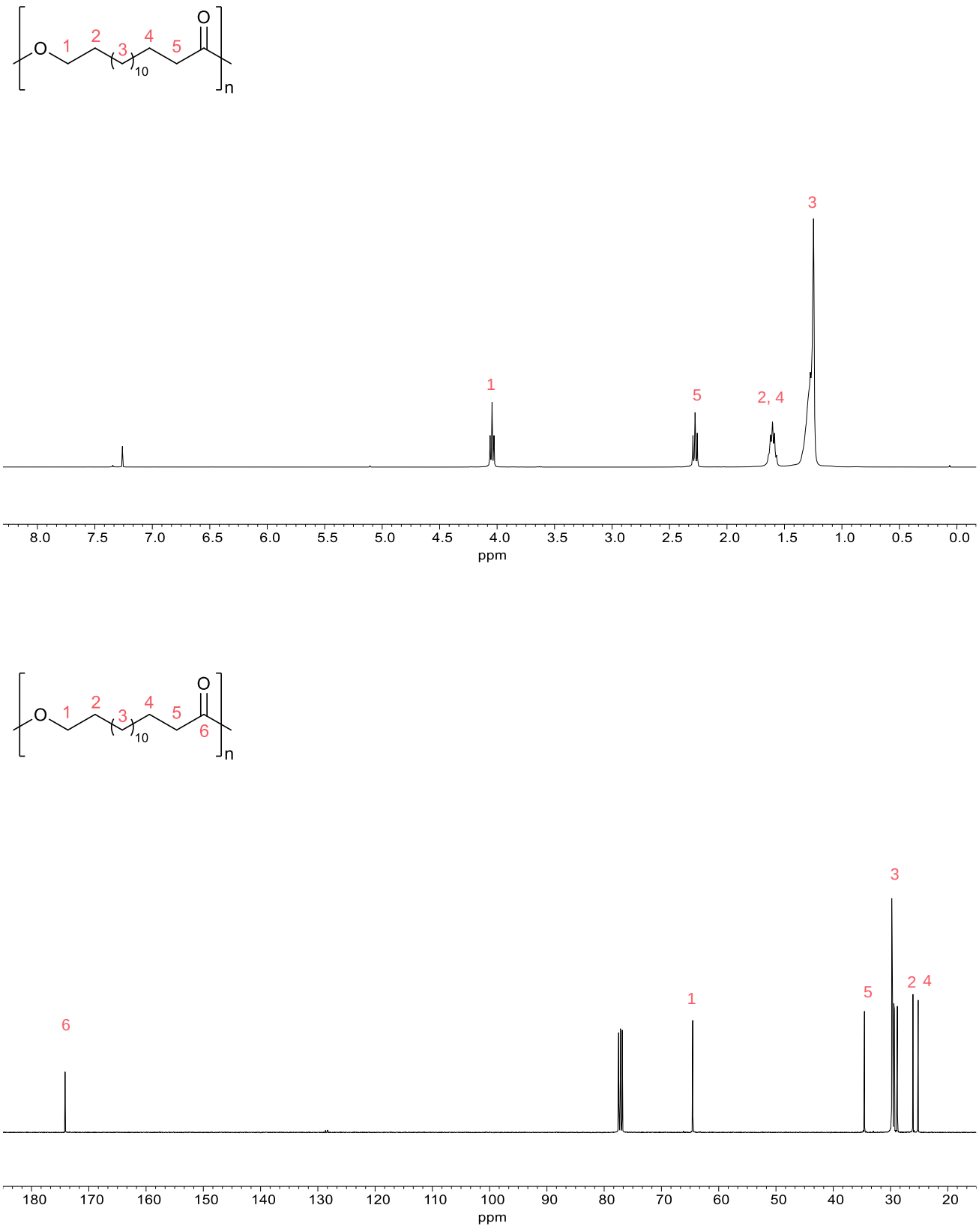


**Fig. S47** $^{1}H$ and $^{13}C\{^{1}H\}$ NMR spectra of polypentadecalactone (PPDL) in $CDCl_3$ at 298 K.

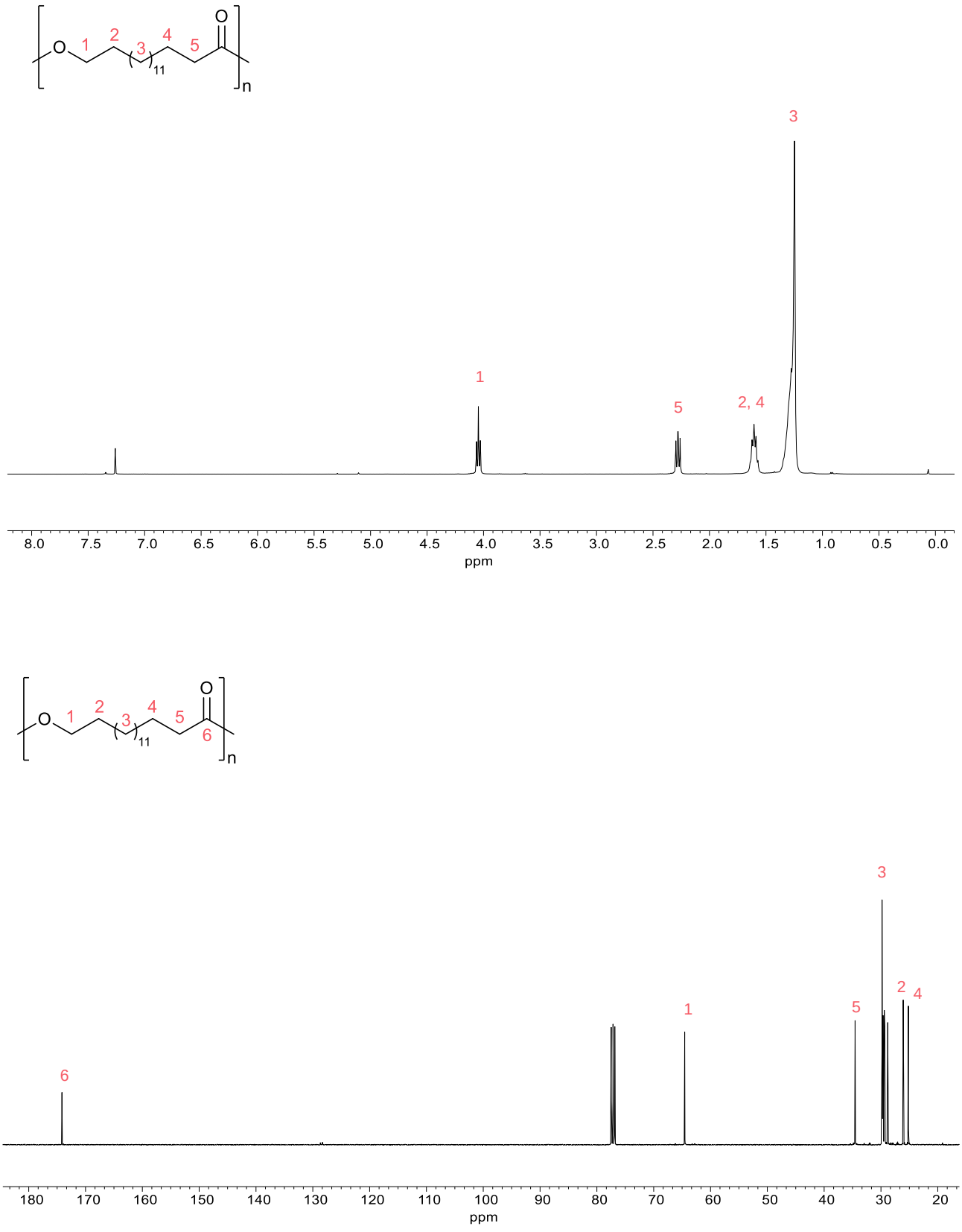


**Fig. S48** $^{1}H$ and $^{13}C\{^{1}H\}$ NMR spectra of polyhexadecalactone (PHDL) in $CDCl_3$ at 298 K.

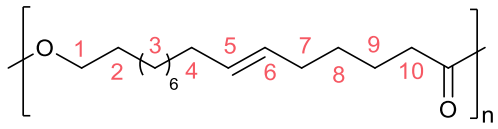


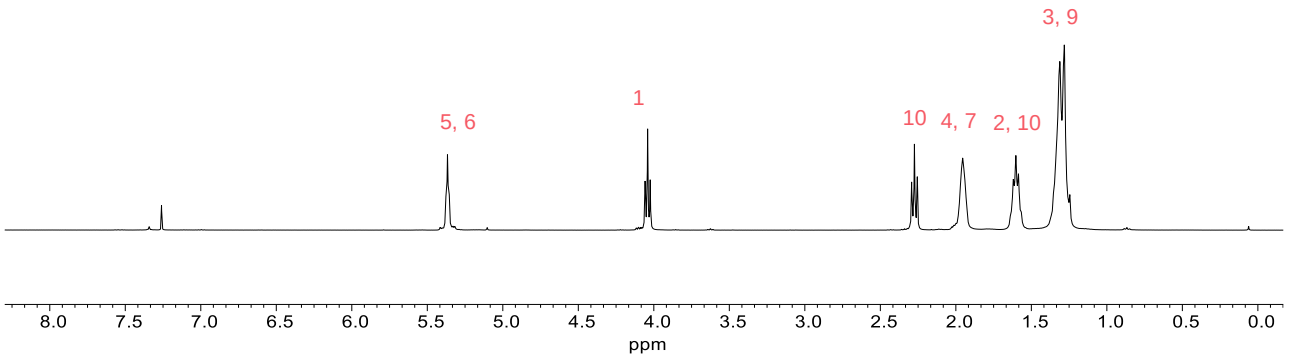


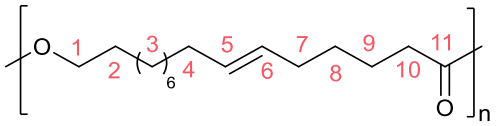


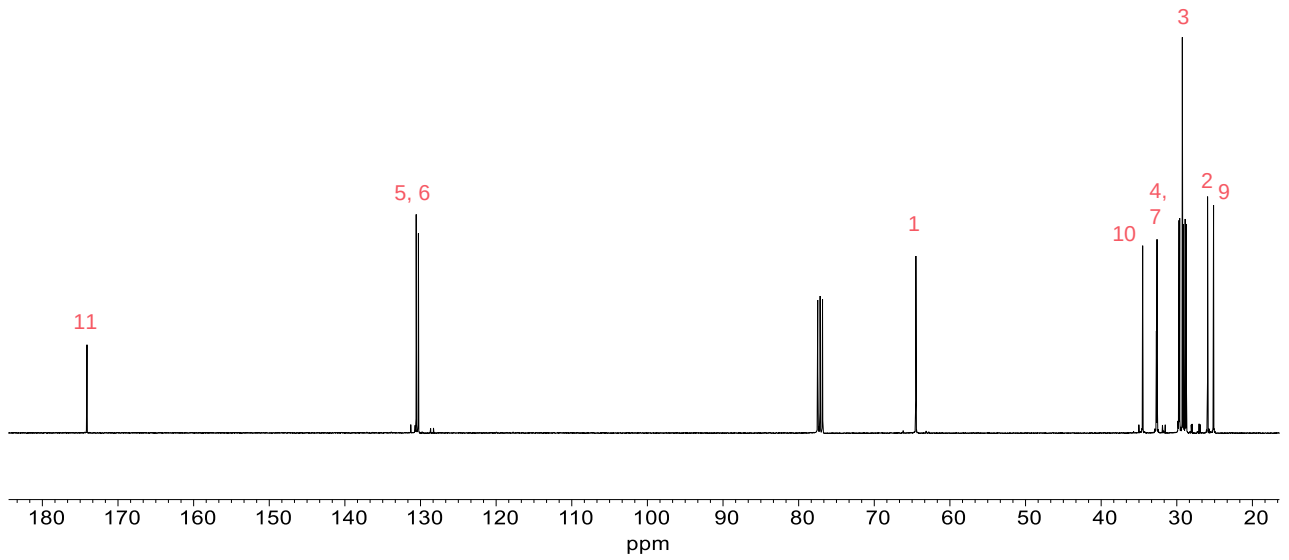


**Fig. S49** $^{1}H$ and $^{13}C\{^{1}H\}$ NMR spectra of poly($\omega$-6-hexadecenlactone, 6HDL) in $CDCl_3$ at 298 K.

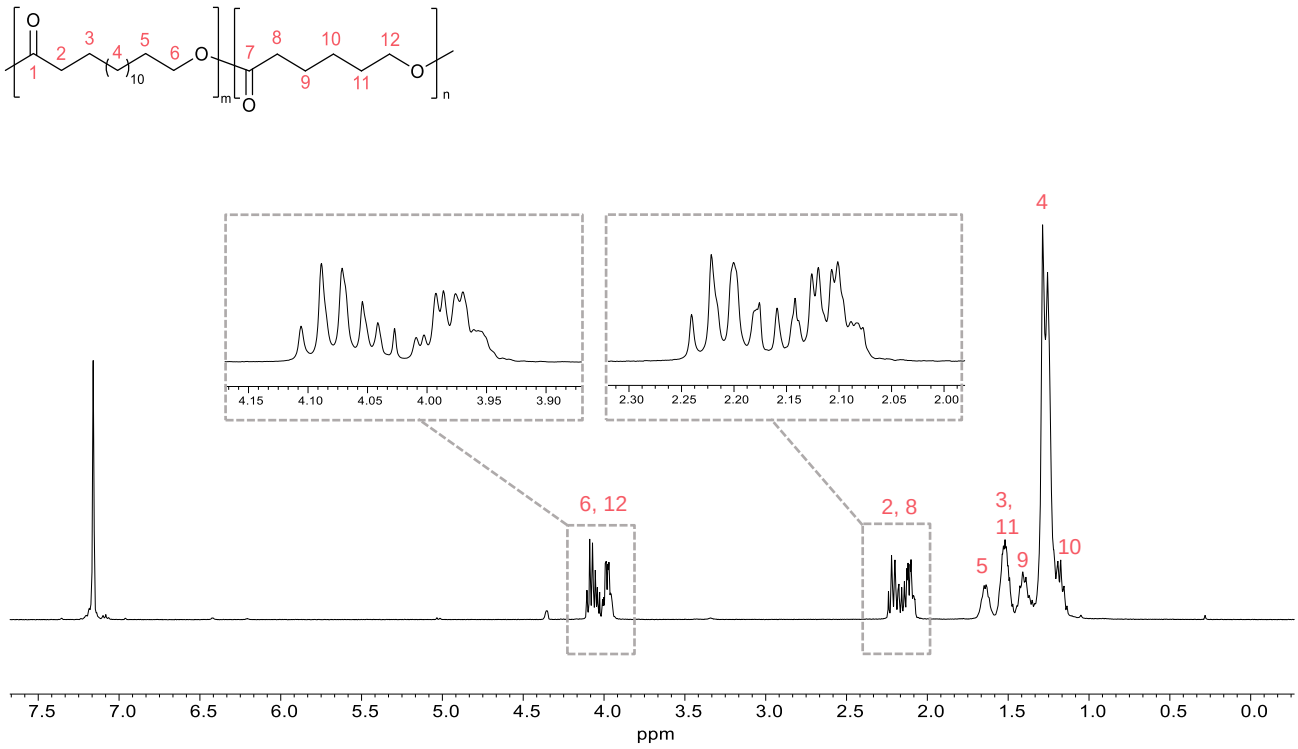


**Fig. S50** $^{1}$H NMR spectrum of poly(PDL-*co*-CL) in $C_6D_6$ at 298 K (Table 4, entry 1).

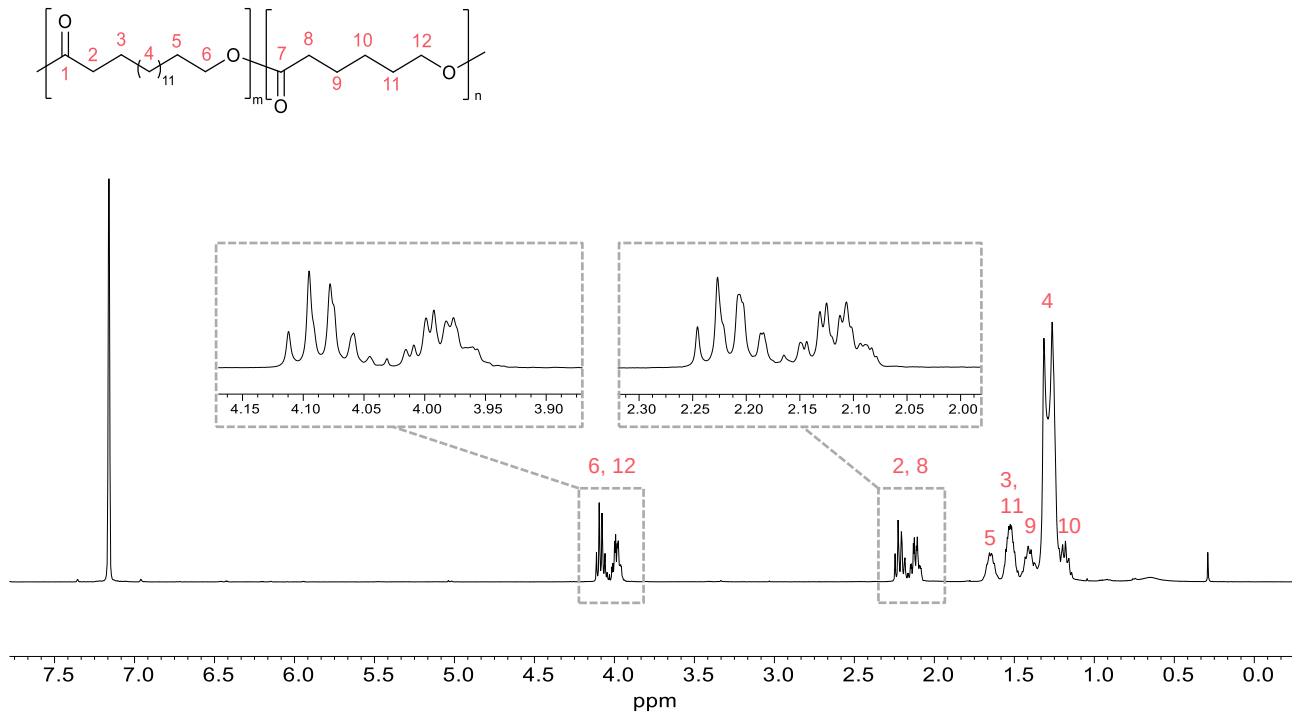


**Fig. S51** $^{1}$H NMR spectrum of poly(HDL-*co*-CL) in $C_6D_6$ at 298 K (Table 4, entry 2).

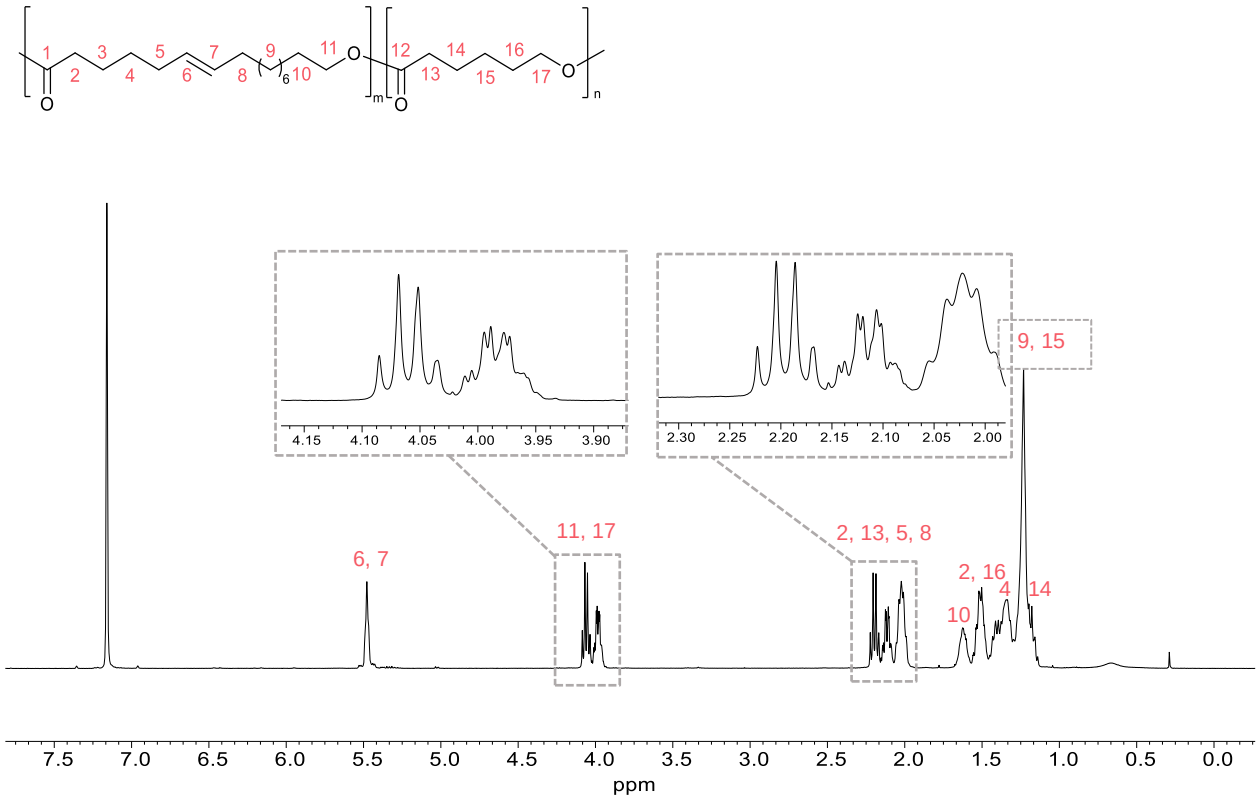


**Fig. S52** $^{1}$H NMR spectrum of poly(6HDL-*co*-CL) in $C_6D_6$ at 298 K (Table 4, entry 3).

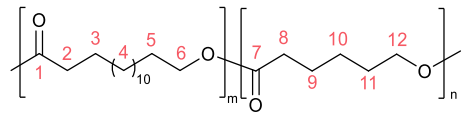


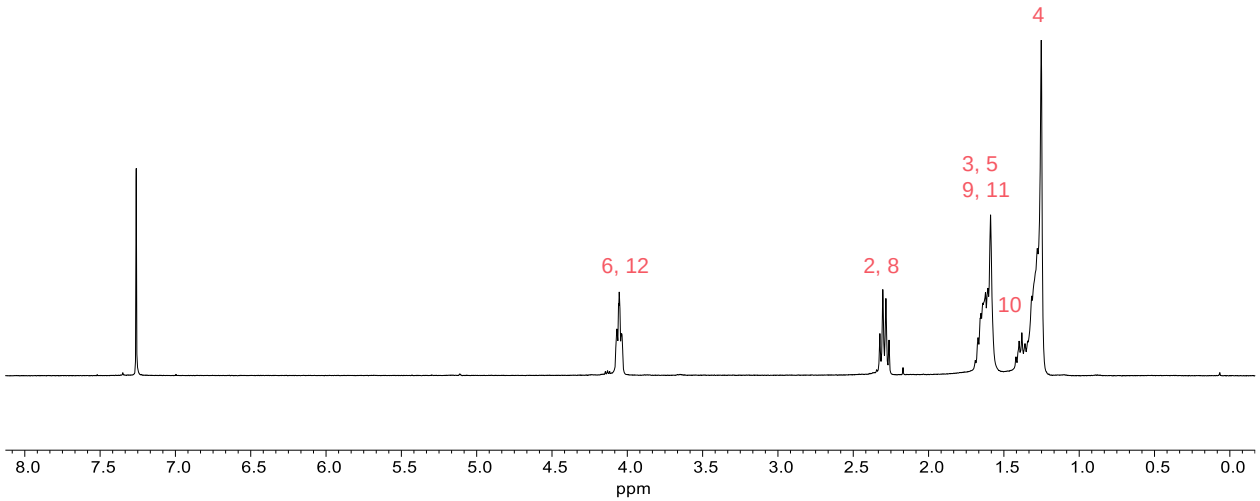


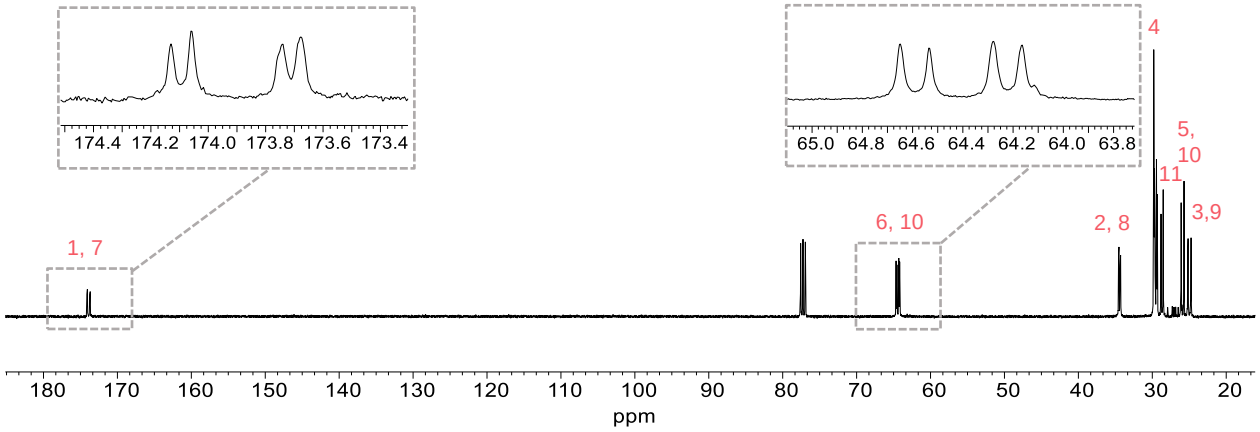


**Fig. S53** $^{1}H$ and $^{13}C\{^{1}H\}$ NMR spectra of poly(PDL-*co*-CL) in $CDCl_3$ at 298 K (Table 4, entry 1).

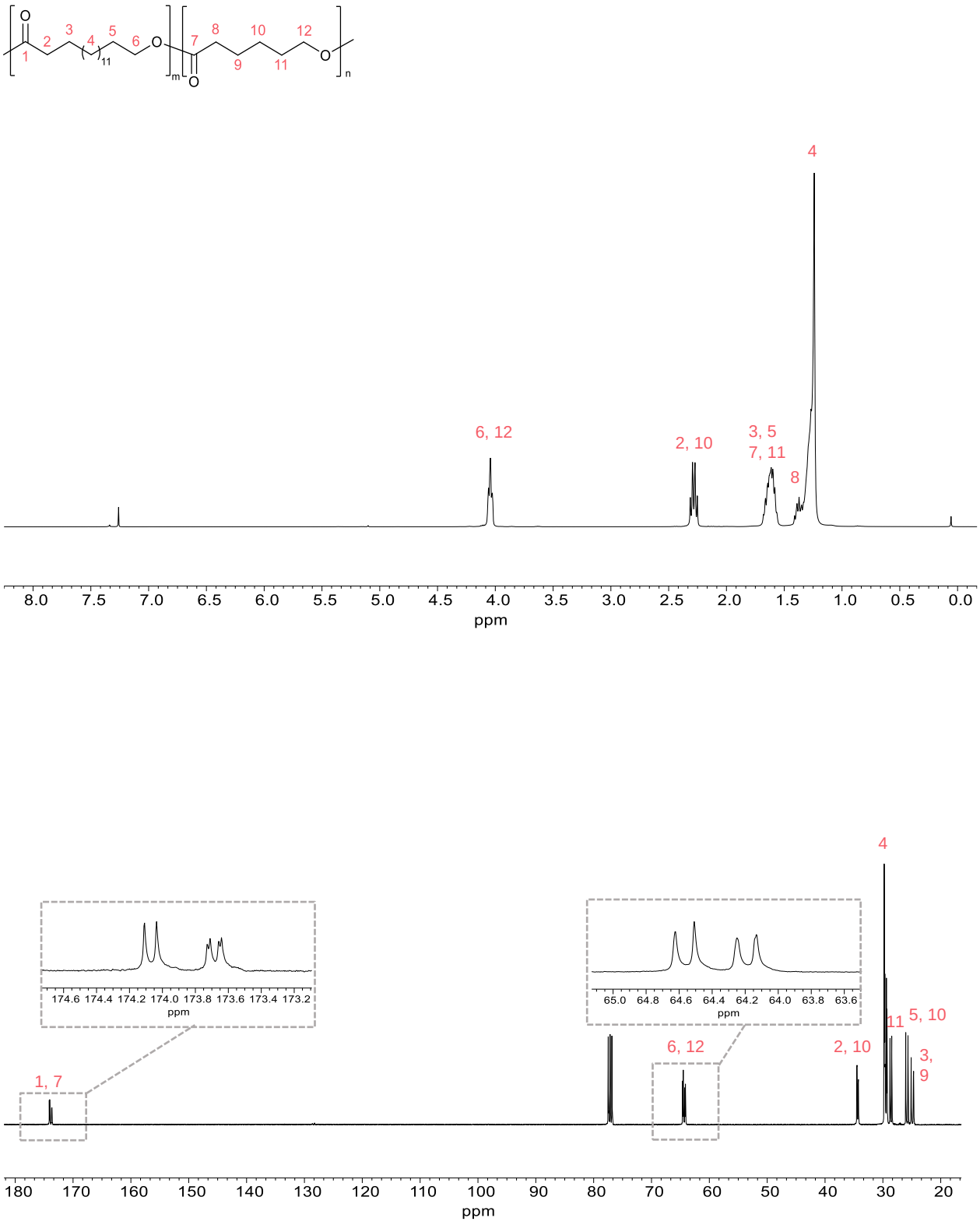


**Fig. S54** $^{1}H$ and $^{13}C\{^{1}H\}$ NMR spectra of poly(HDL-*co*-CL) in $CDCl_3$ at 298 K (Table 4, entry 2).

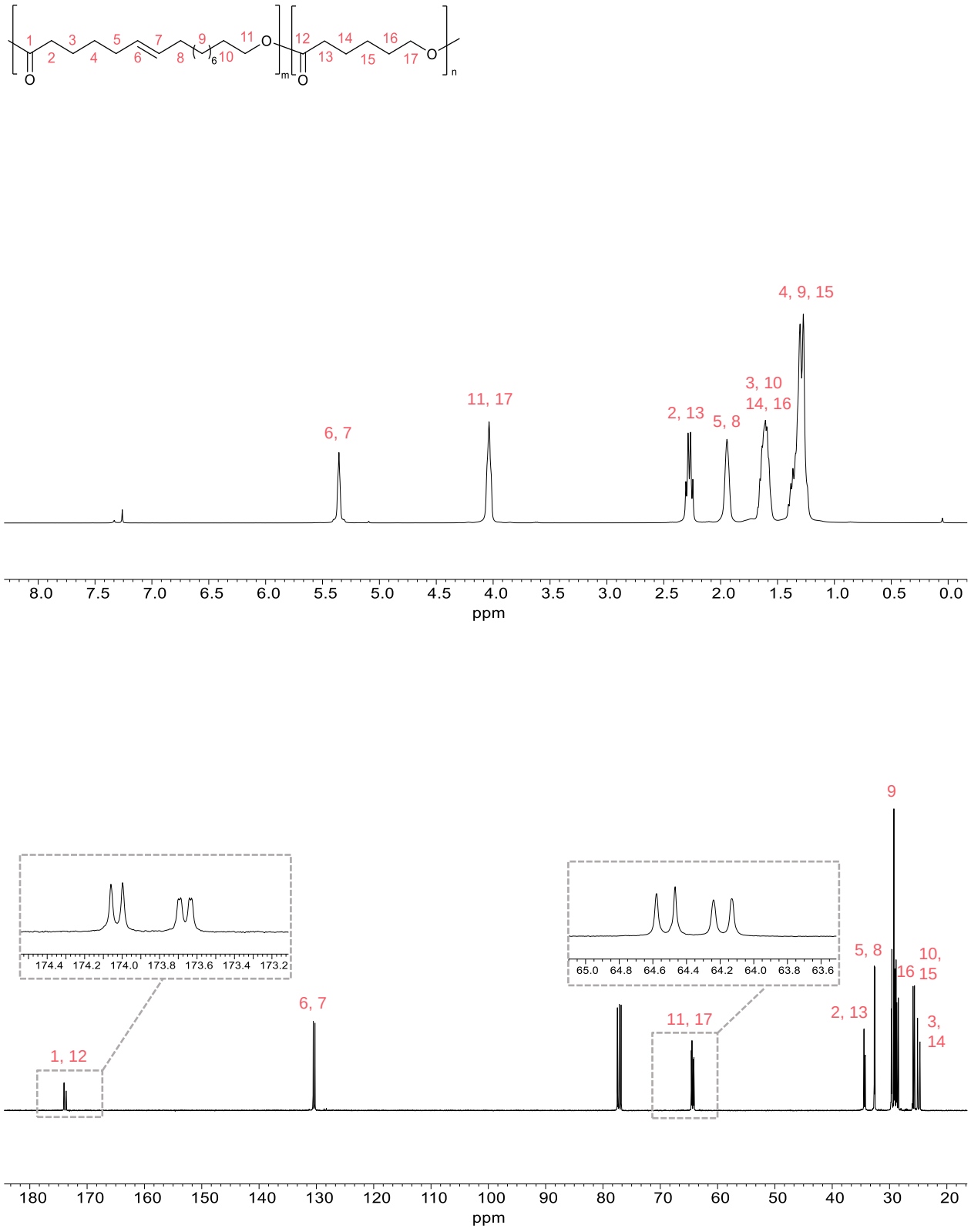


**Fig. S55** $^{1}H$ and $^{13}C\{^{1}H\}$ NMR spectra of poly(6HDL-*co*-CL) in $CDCl_3$ at 298 K (Table 4, entry 3).

**Sequential monomer addition**

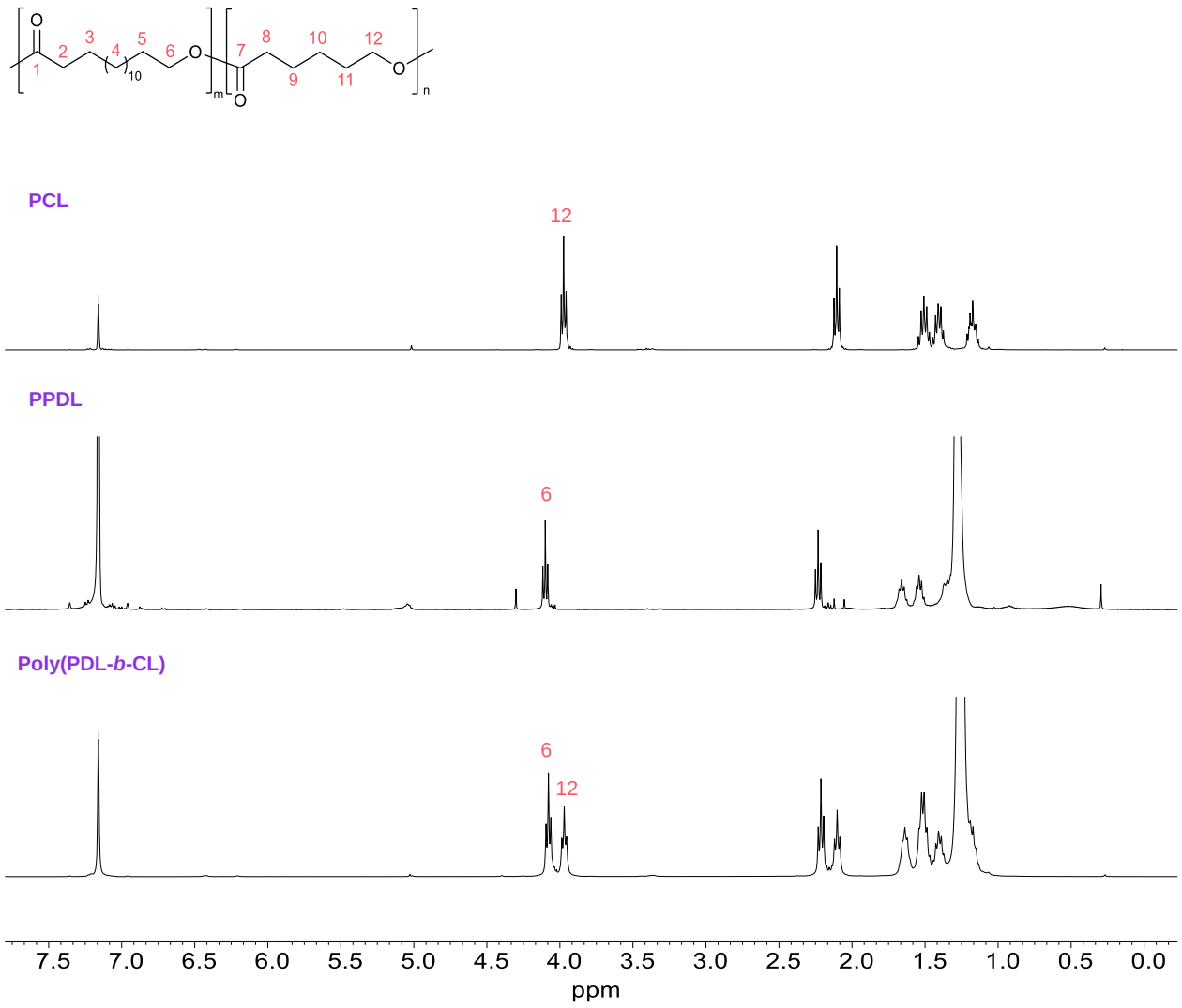


**Fig. S56** $^{1}$H NMR spectra of poly(PDL-*b*-CL) in $C_6D_6$ at 298 K.

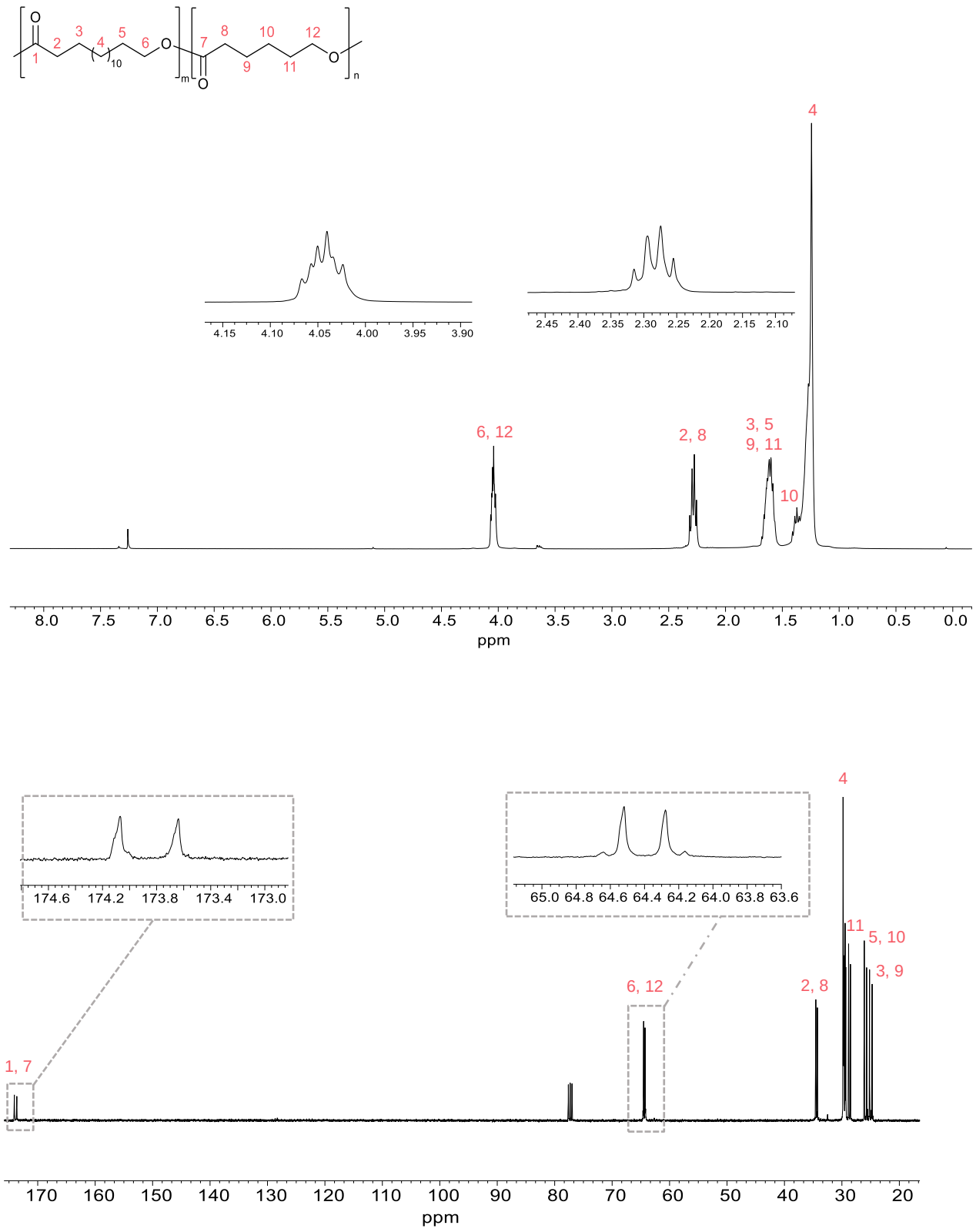


**Fig. S57** $^{1}H$ and $^{13}C\{^{1}H\}$ NMR spectra of poly(PDL-*b*-CL) in $CDCl_3$ at 298 K (Table 4, entry 4).

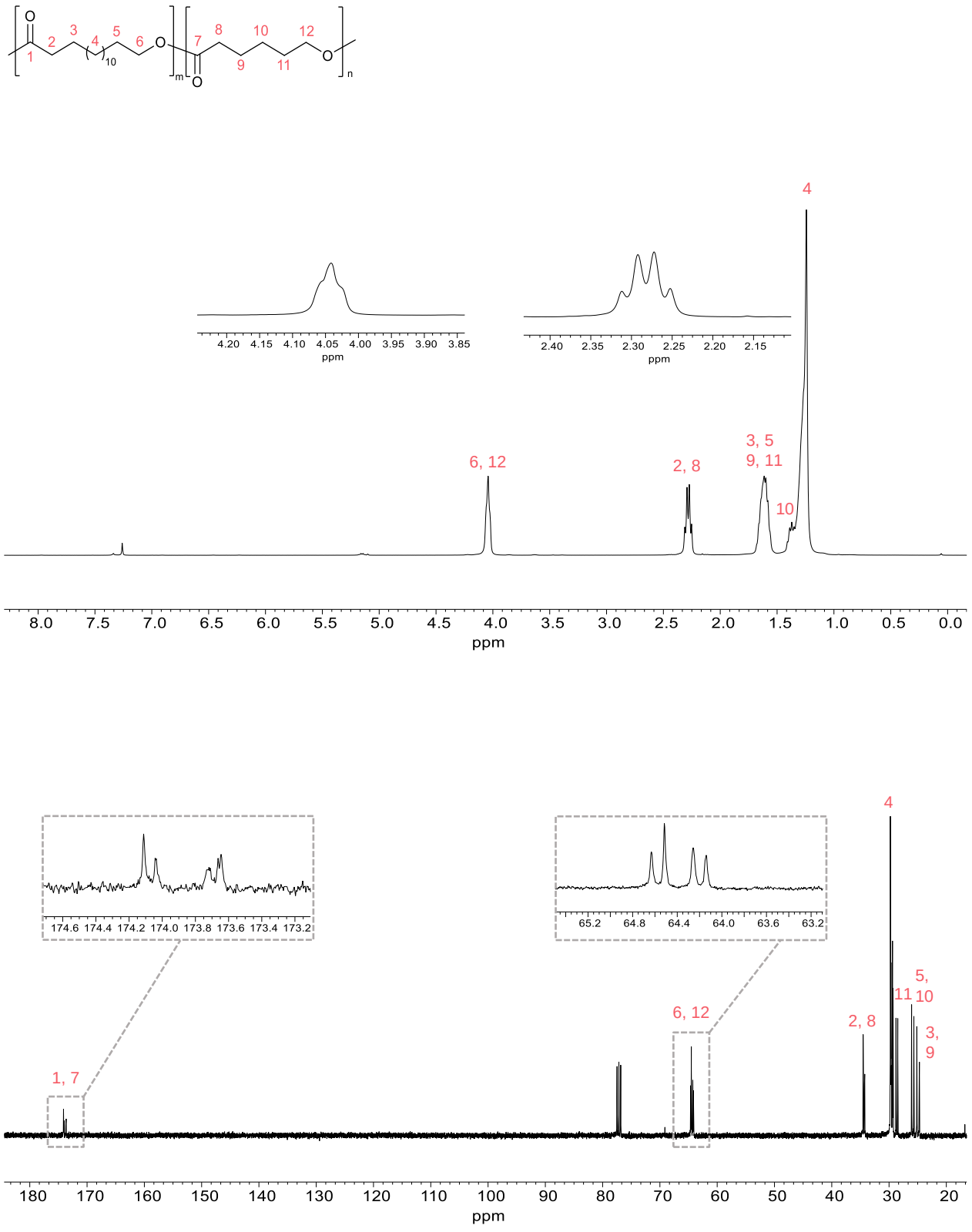


**Fig. S58** $^{1}H$ and $^{13}C\{^{1}H\}$ NMR spectra of poly(PDL-*co*-CL) in $CDCl_3$ at 298 K (Table 4, entry 5).

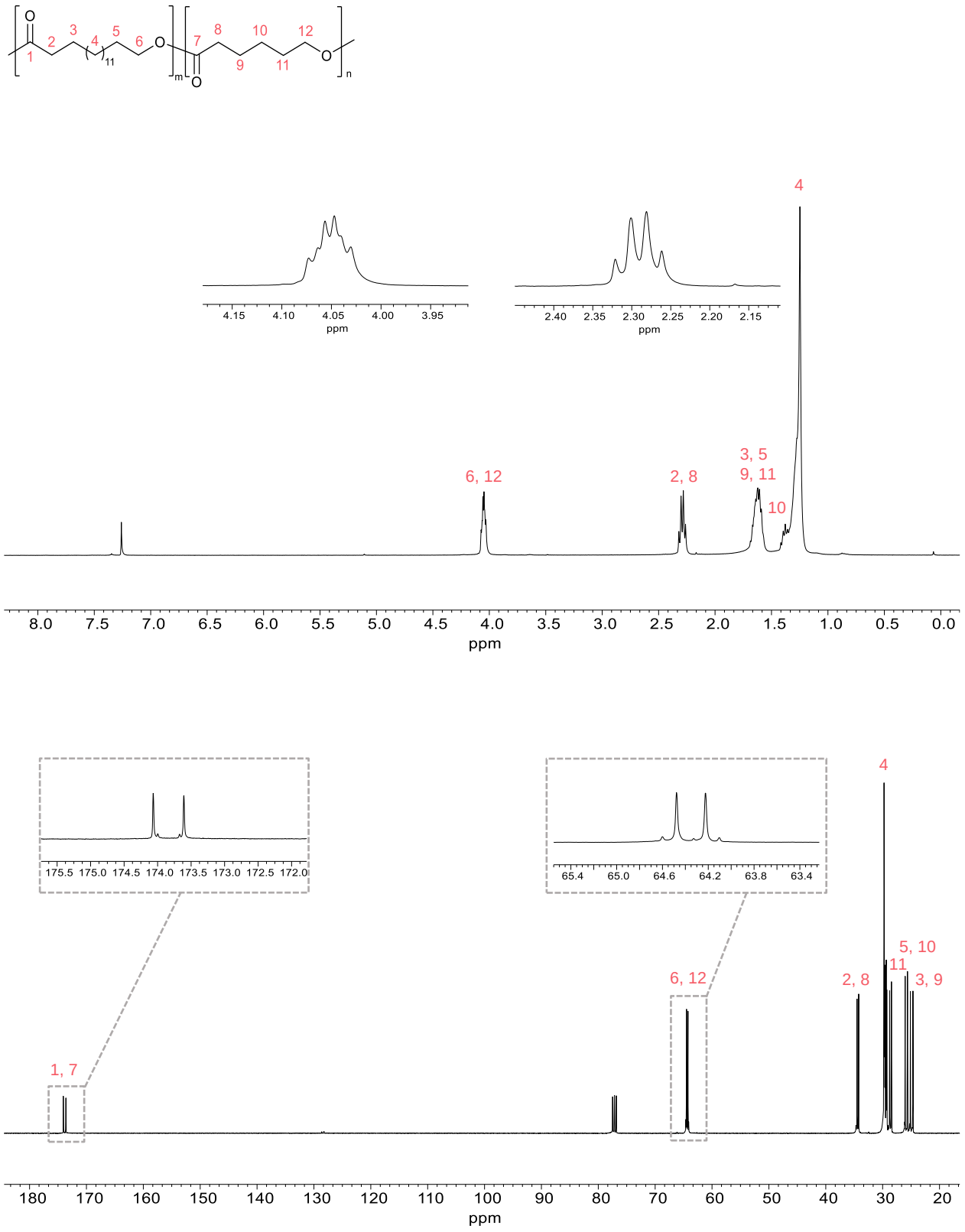


**Fig. S59** $^{1}H$ and $^{13}C\{^{1}H\}$ NMR spectra of poly(HDL-*b*-CL) in $CDCl_3$ at 298 K (Table 4, entry 6).

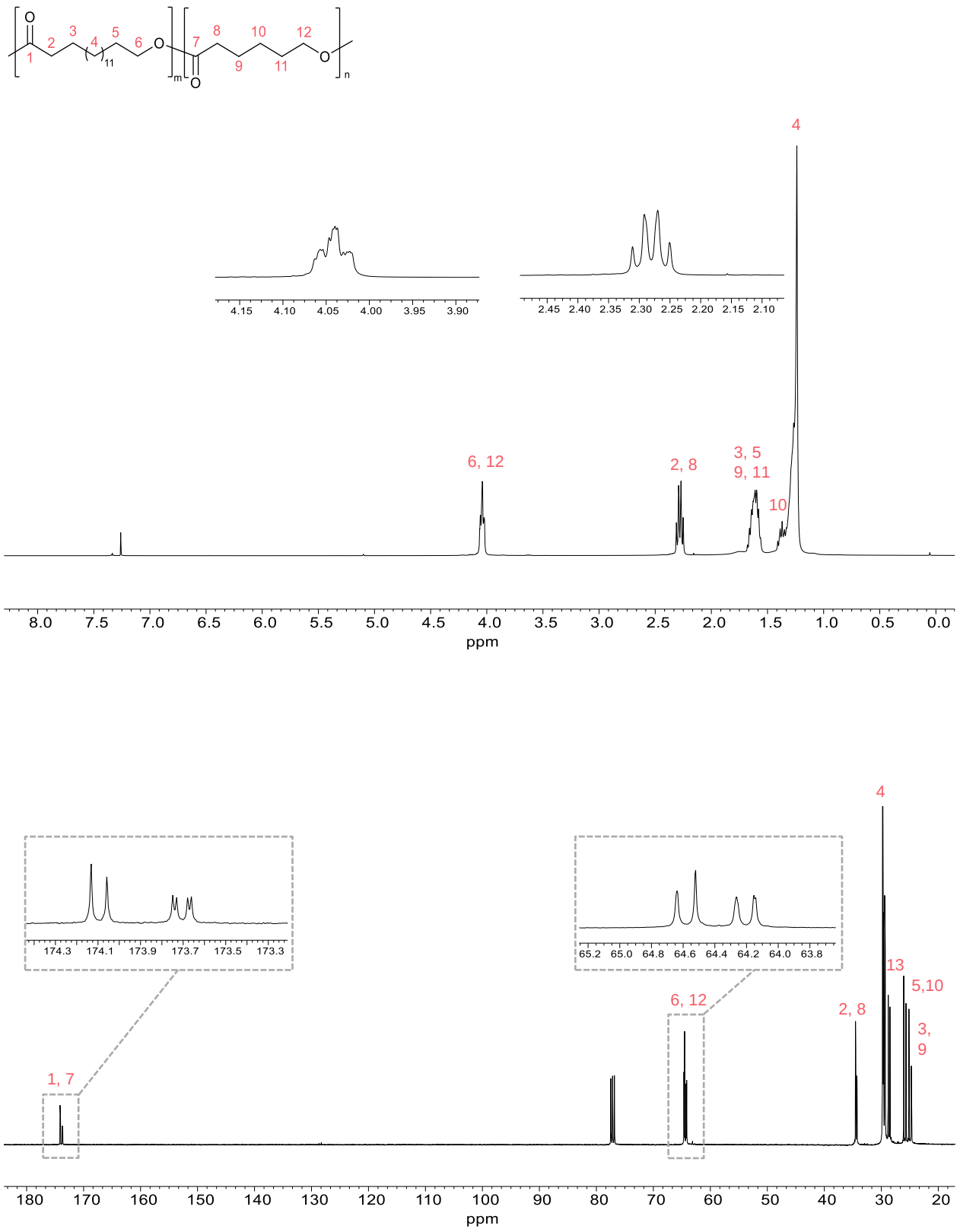


**Fig. S60** $^{1}H$ and $^{13}C\{^{1}H\}$ NMR spectra of poly(HDL-*co*-CL) in $CDCl_3$ at 298 K (Table 4, entry 7).

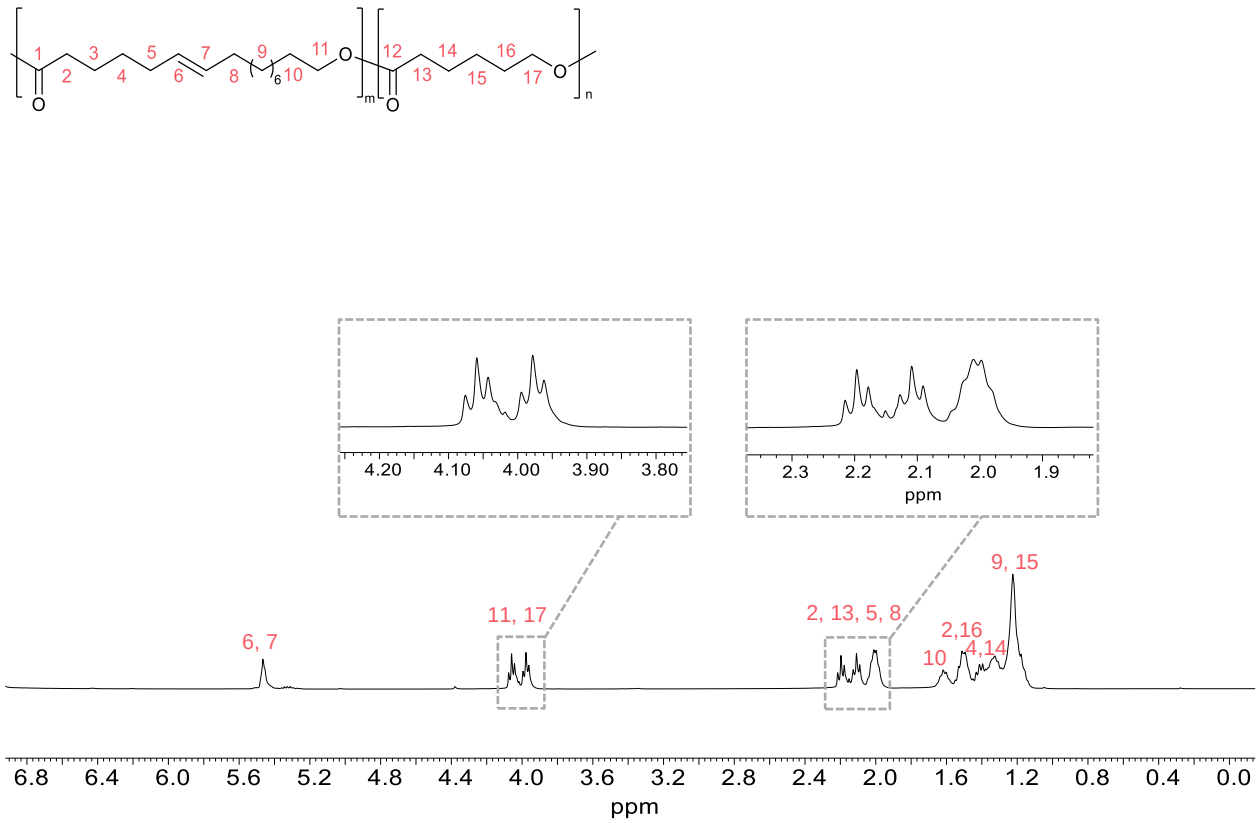


**Fig. S61** $^{1}$H NMR spectrum of poly(6HDL-*b*-CL) in $C_6D_6$ at 298 K (Table 4, entry 8).

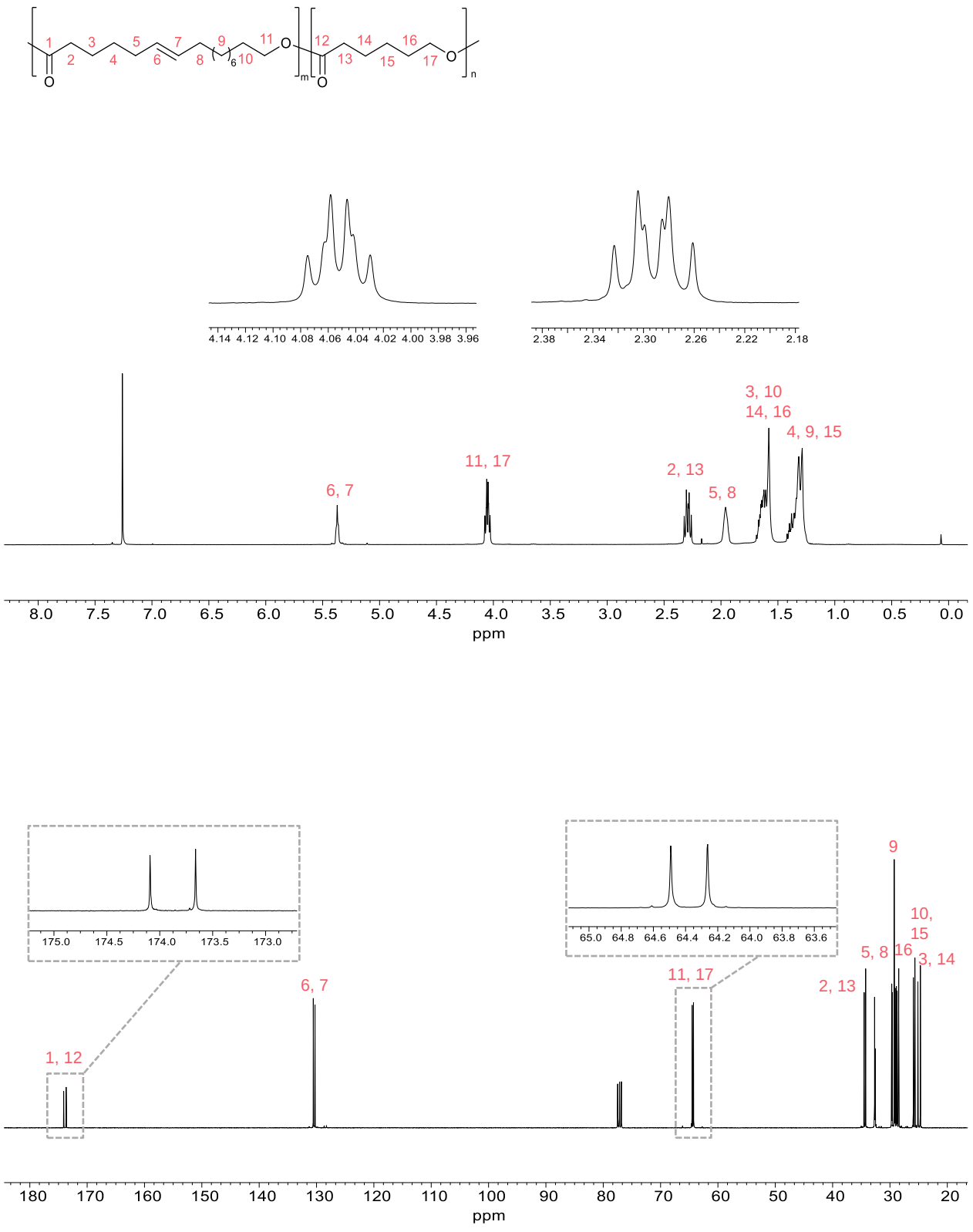


**Fig. S62** $^{1}H$ and $^{13}C\{^{1}H\}$ NMR spectra of poly(6HDL-*b*-CL) in $CDCl_3$ at 298 K (Table 4, entry 8).

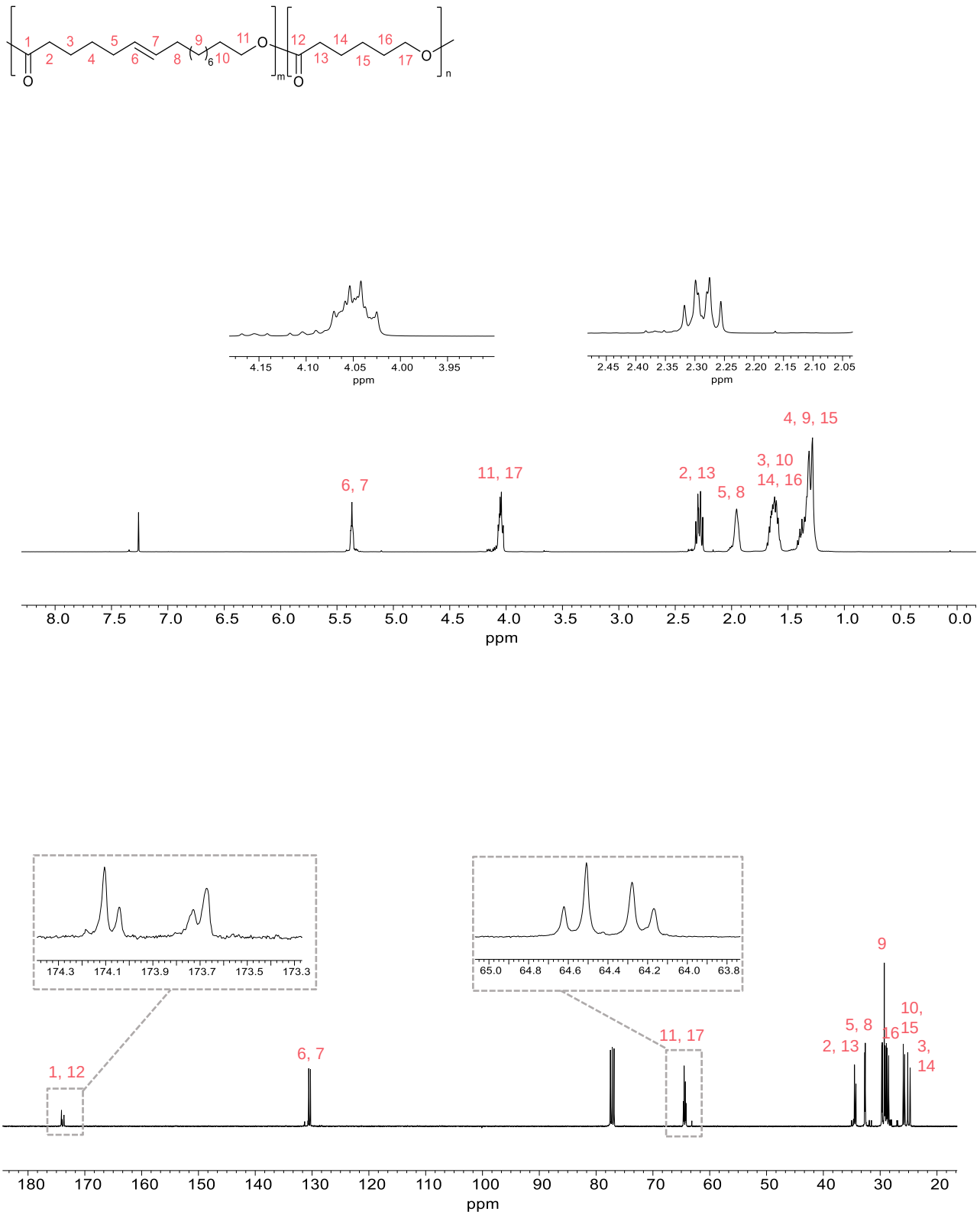


**Fig. S63** $^{1}H$ and $^{13}C\{^{1}H\}$ NMR spectra of poly(6HDL-*co*-CL) in $CDCl_3$ at 298 K (Table 4, entry 9).

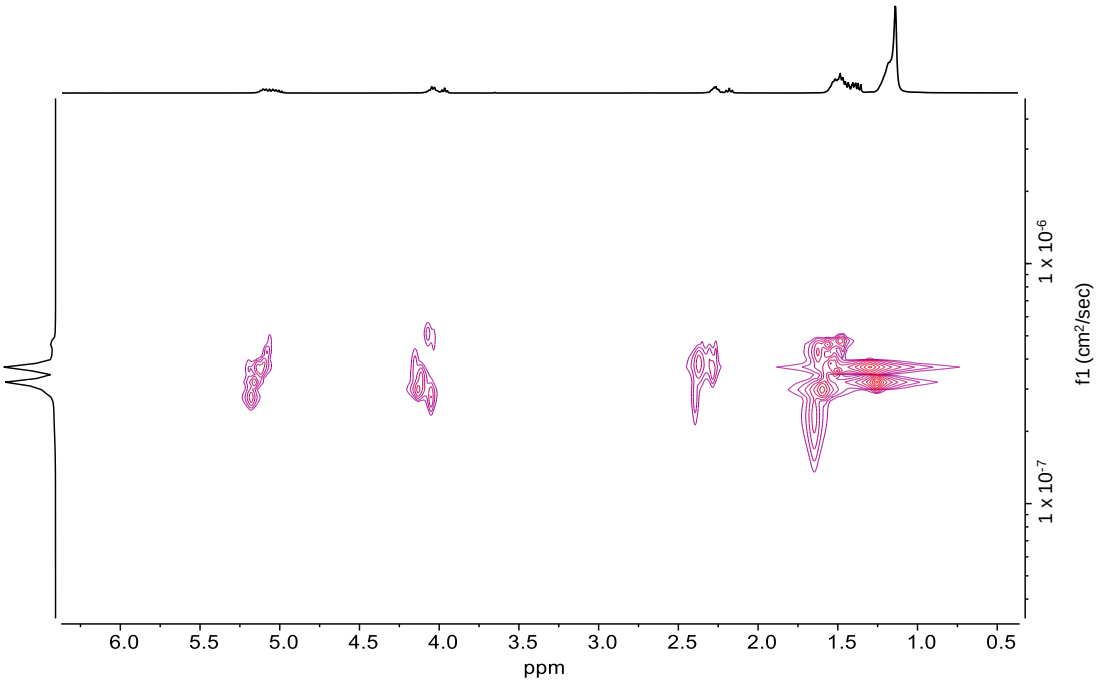


**Fig. S64** The DOSY NMR spectrum of a poly(PDL-*co*-L-LA) in $CDCl_3$ (Table 6, entry 2).

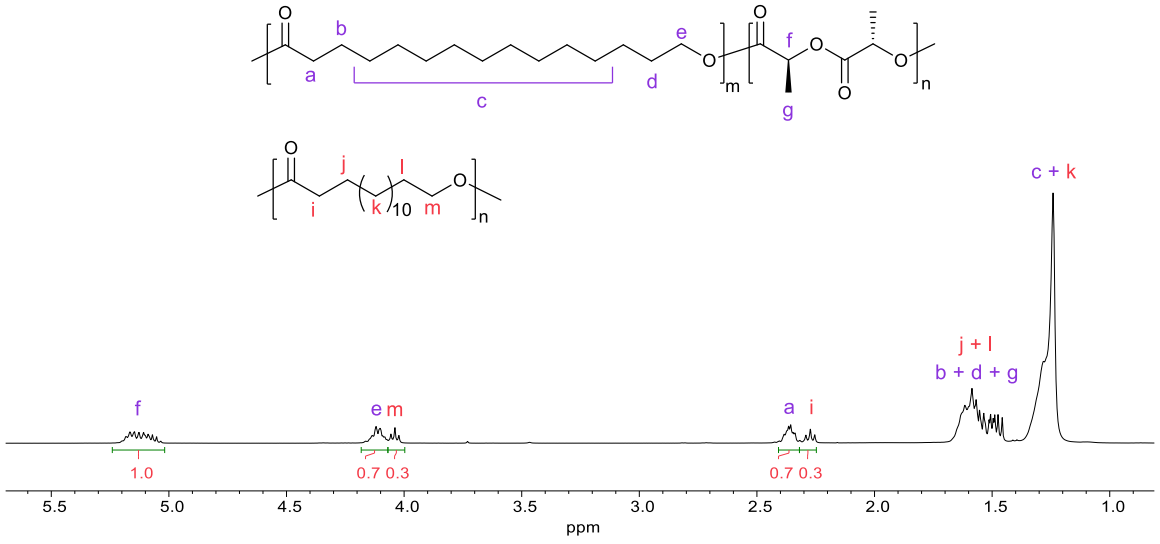


**Fig. S65** $^1$H NMR spectrum of poly(L-LA-*co*- PDL) (Table 6, entry 3).

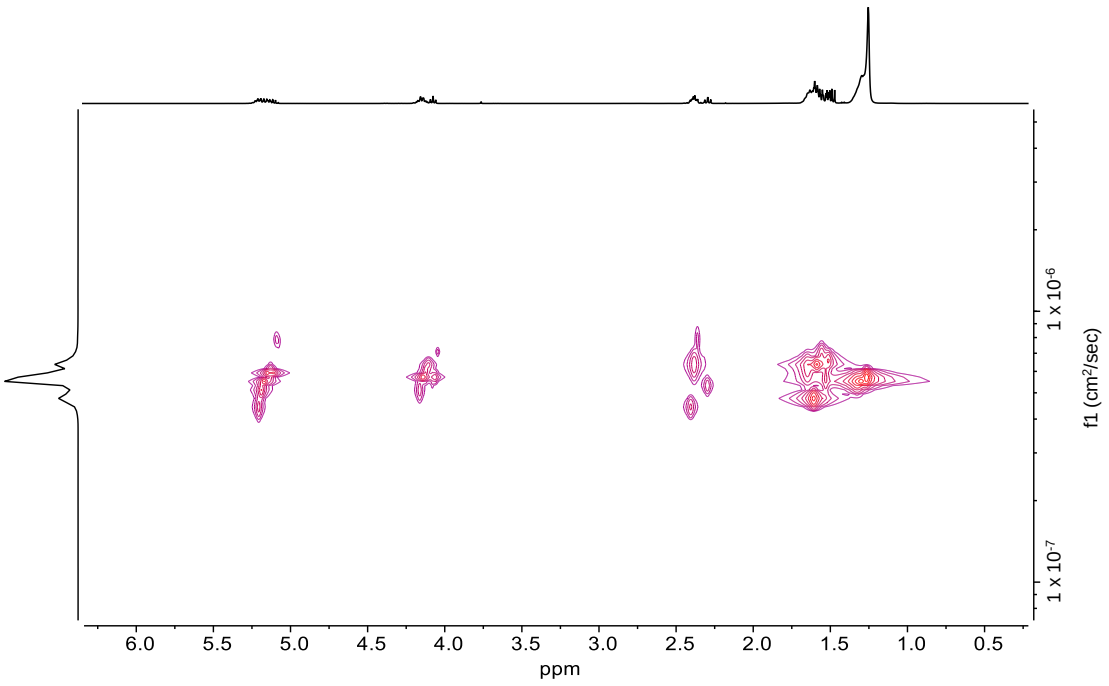


**Fig. S66** The DOSY NMR spectrum of a poly(L-LA-*co*- PDL) in $CDCl_3$ (Table 6, entry 3).

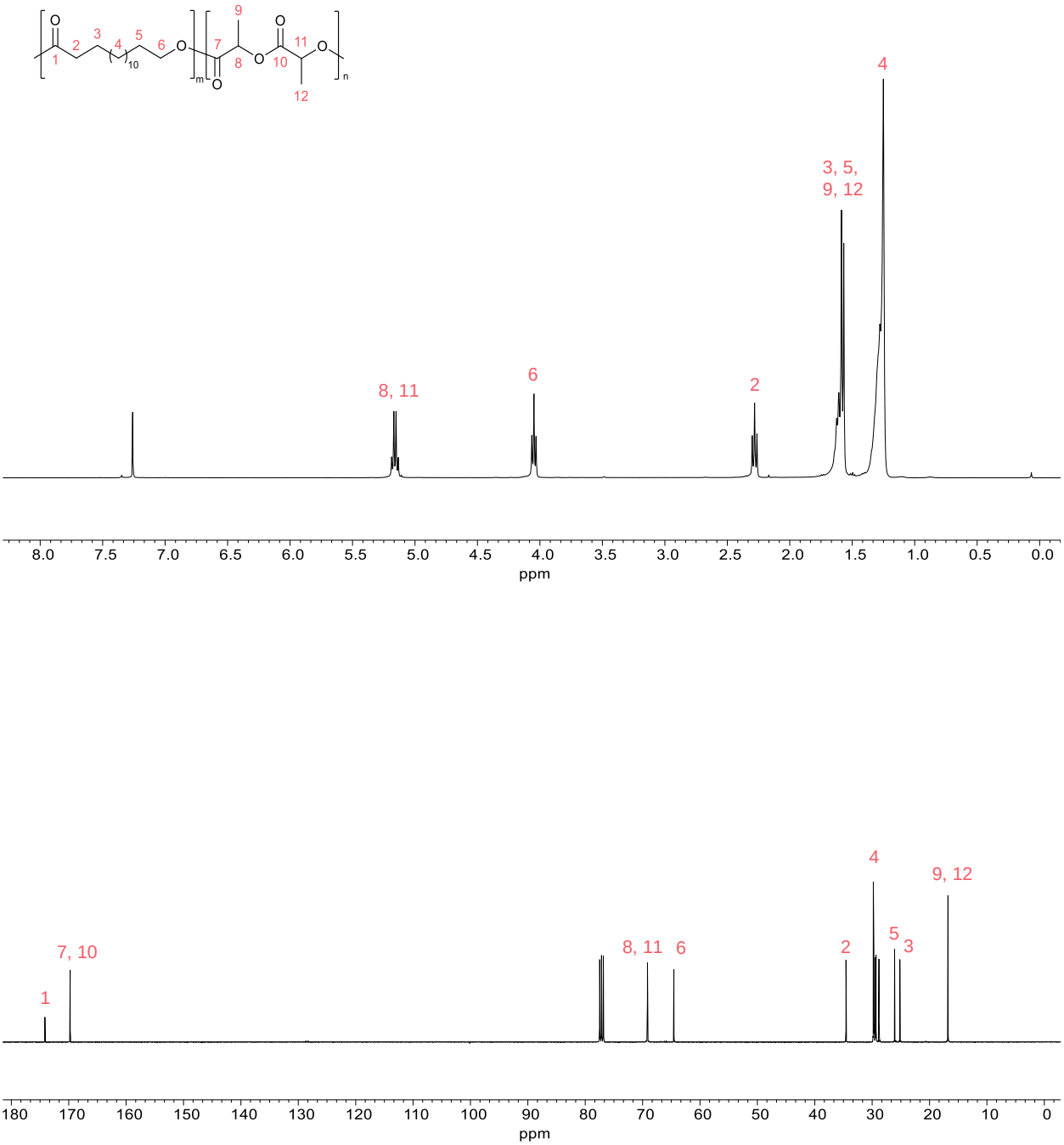


**Fig. S67** $^{1}H$ and $^{13}C\{^{1}H\}$ NMR spectra of poly(L-LA-*b*-PDL) in $CDCl_3$ at 298 K (Table 6, entry 1).

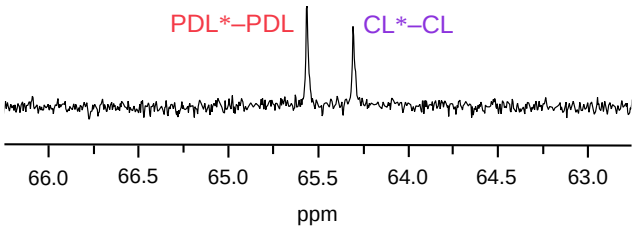


**Fig. S68** $^{13}C\{^{1}H\}$ NMR spectra at the methylene region of poly(PDL-*b*-CL) in $CDCl_3$ at 298 K (Table 7, entry 1).

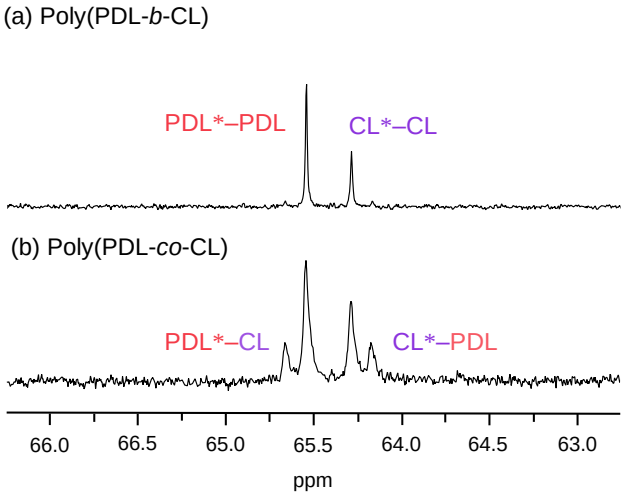


**Fig. S69**$^{13}C\{^{1}H\}$ NMR spectra at the methylene region of poly(PDL-*b*-CL) (**a**, 30 + 5 min) and (**b**, 30 + 360 min) poly(PDL-*co*-CL) in $CDCl_3$ at 298 K (Table 7, entry 2).

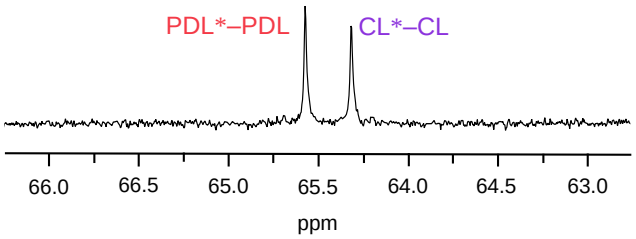


**Fig. S70** $^{13}C\{^{1}H\}$ NMR spectra at the methylene region of poly(PDL-*b*-CL) in $CDCl_3$ at 298 K (Table 7, entry 3).

## Ring-Opening Polymerization of L-LA using complexes 1–10

The polymerizations of high ring strain L-lactide (L-LA) were also carried out in order to compare the results with the polymerizations of MLs (Table S1). The values of the apparent rate constants ($k_{app}$) collected in Table S1 show that the catalytic activity decreases in the order **5** > **7** > **4** > **6** > **9** ≈ **10** > **8** > **2** > **1** > **3**. Complex **5**, featuring electron-withdrawing iodo atoms, was the most active catalyst examined in this study. Despite its acknowledged significance, complex **5** is the most active aluminum salen catalyst reported thus far. A smaller, although substantial, rate enhancement was also seen upon replacing a phenyl with a naphthalene ring (complex **4** vs. complex **7**). However, complex **6** with the electron withdrawing $NO_2$ groups ($k_{app}$ = (176 ± 7.77) × $10^{-5}$ $s^{-1}$) displayed lower catalytic activity than the unsubstituted complex **4** ($k_{app}$ = (226 ± 6.59) × $10^{-5}$ $s^{-1}$). The observed lower catalytic activity in complex **6** may be attributed to the stronger binding of the ring-opened alkoxide chain to the more Lewis acidic aluminum center that hinders the subsequent insertion step.[1-4] For the *bis*(pyrrolidene) aluminum complexes **9** and **10**, the similar $k_{app}$ values were observed ($k_{app}$ = (51.00 ± 2.70) × $10^{-5}$ $s^{-1}$ for **9**[55] and $k_{app}$ = (52.29 ± 2.64) × $10^{-5}$ $s^{-1}$ for **10**), indicating that the steric effect was not evidenced in this group. It can be observed that the tetradentate aluminum complexes with the gem-dimethyl-substituted propylene backbone (**4**–**7** and **9**–**10**) exhibited higher catalytic performance than tetradentate aluminum complexes with ethylene linker (complexes **3** and **8**). The observed higher catalytic activity could be attributed to the greater flexibility of the 2,2-dimethylpropylene backbone imparted to the metal coordination sphere and hence better accommodation of the geometric requirements of the transition states for the ring-opening process.[5] In addition, changing the backbone from a $C_2$ alkylene linker to a $C_3$ unit results in a change in the conformation from *meridional* to *facial*.[6] The *facial* conformation is more reactive because there is more space for the monomer to coordinate *cis* to the growing polymer chain, which is required for the insertion step. Similar to the polymerization of MLs, the low coordinate bidentate aluminum complexes **1** and **2** displayed lower activity than the high coordinate tetradentate ones.[7,8]

**Table S1** Kinetic results for the ROP of MLs and L-LA using aluminum complexes **1**–**10** in the presence of benzyl alcohol.[a]

| Entry | Complex | $k_{app}$ ($10^{-5}$ $s^{-1}$) |
|---|---|---|
| 1 | **1** | 9.19 ± 0.23 |
| 2 | **2** | 16.96 ± 0.76 |
| 3 | **3** | 6.85 ± 0.27 |
| 4 | **4** | 226 ± 6.59 |
| 5 | **5** | 1288 ± 55.46 |
| 6 | **6** | 176 ± 7.77 |
| 7 | **7** | 463 ± 20.07 |
| 8 | **8** | 33.82 ± 0.92 |
| 9 | **9** | 51.00 ± 2.70[9] |
| 10 | **10** | 52.29 ± 2.64 |

[a][L-LA]$_0$:[Al]:[BnOH] = 50, [L-LA]$_0$ = 0.42 M, [Al] = 8.33 mM, toluene, 70 ºC.

## References


[1] K. Ding, M. O. Miranda, B. Moscata-Goodpaster, N. Ajellal, L. E. Breyfogle, E. D. Hermes, C. P. Schaller, S. E. Roe, C. J. Cramer, M. A. Hillmyer and W. B. Tolman, *Macromolecules*, 2012, **45**, 5387–5396.

[2] S. Bian, S. Abbina, Z. Lu, E. Kolodka and G. Du, *Organometallics*, 2014, **33**, 2489–2495.

[3] S. Kamavivhanurat, K. Jampakaew and P. Hormnirun, *Polym. Chem.* 2023, **14**, 1752–1772.

[4] C. Nakonkhet, T. Nanok, P. Chuawong, W. Wattanathana and P. Hormnirun, *Dalton Trans.*, 2017, **46**, 11013−11030.

[5] P. Hormnirun, E. L. Marshall, V. C. Gibson, R. I. Pugh and A. J. P. White, *Proc. Natl. Acad. Sci.*, 2006, **103**, 15343–15348.

[6] M. P. F. Pepels, M. Bouyahyi, A. Heise, and R. Duchateau, *Macromolecules*, 2013, **46**, 4324−4334.

[7] Y. Liu, W.-S. Dong, J.-Y. Liu and Y.-S. Li, *Dalton Trans.*, 2014, **43**, 2244–2251.

[8] H.-C. Huang, B. Wang, Y.-P. Zhang and Y.-S. Li, *Polym. Chem.*, 2016, **7**, 5819−5827.

[9] S. Tabthong, T. Nanok, P. Sumrit, P. Kongsaeree, S. Prabpai, P. Chuawong and P. Hormnirun, *Macromolecules*, 2015, **48**, 6846–6861.